

Experimental investigation on the effects of channel material, size, and oil viscosity in horizontal mini-channels

by

Kevin Kombo Bultongez

B.S., Kansas State University, 2015

A THESIS

submitted in partial fulfillment of the requirements for the degree

MASTER OF SCIENCE

Department of Mechanical and Nuclear Engineering  
College of Engineering

KANSAS STATE UNIVERSITY  
Manhattan, Kansas

2017

Approved by:

Major Professor  
Melanie M. Derby

# Copyright

© Kevin Bultongez 2017.

## Abstract

Oil-water separation is an important process in the petroleum industry. This research investigates the use of surface tension forces to improve current oil-water separation technologies; an understanding of oil-water flows in surface tension driven mini-channels is a necessary first step. This work investigates the effects of mini-channel tube diameter, wall material, and oil viscosity on flow regimes and pressure drops in mini-channel oil-water flows. A horizontal closed-loop, adiabatic experimental apparatus was constructed and validated using single-phase water. Experiments tested 2.1-mm and 3.7-mm borosilicate glass, 3.7-mm stainless steel and 4.0-mm Inconel tubes, resulting in Eötvös numbers of 0.2, 0.6 and 0.7. The experimental data were analyzed and compared using two mineral oils (i.e., Parol 70 and 100) with densities of  $840 \text{ kg/m}^3$  for both and viscosities of 11.7 and 20.8 mPa-s, respectively. Experiments included a wide range of oil superficial velocities (e.g., 0.28–6.82 m/s for glass, 0.28–2.80 m/s for stainless steel and 0.21–2.89 for Inconel) and water superficial velocities (e.g., 0.07–6.77 for glass, 0.07–4.20 m/s for stainless steel and 0.06–3.86 m/s for Inconel). Flow regimes were observed and classified as stratified, annular, intermittent, and dispersed flow regimes. Effects of tube diameter were observed. For example, the 2.1-mm glass tube had the smaller range of stratified flows and the largest range of annular and intermittent flows compared to the 3.7-mm glass tube. At the same oil and water superficial velocities and relatively the same flow regime, stainless steel and Inconel always displayed higher pressure drop than the glass tube. However, pressure drops were a strong function of flow regime; lowest pressure drops were found for annular flows and highest pressure drops for dispersed flows. Flow regime maps were created and pressure drops quantified. Overall effects of oil viscosity were modest; however, an increase in oil viscosity enhanced flow stability which affected flow regime transition points.

## Table of Contents

List of Figures .....	v
List of Tables .....	vi
Acknowledgements .....	vii
Chapter 1 - INTRODUCTION .....	1
Chapter 2 - LITERATURE REVIEW .....	3
Chapter 3 - EXPERIMENTAL DESIGN .....	13
Chapter 4 - RESULTS AND DISCUSSION .....	26
Chapter 5 - CONCLUSIONS AND FUTURE WORK .....	57
References .....	61
Appendix A - Fluid Properties .....	64

## List of Figures

Figure 1 Experimental apparatus .....	14
Figure 2 Test section.....	15
Figure 3 Single-phase water pressure drop on borosilicate glass tube A) 2.1 mm B) 3.7 mm.....	23
Figure 4 Stratified flow regime.....	29
Figure 5 Annular flow regime.....	30
Figure 6 Intermittent flow regime.....	31
Figure 7 Dispersed flow.....	32
Figure 8 Flow regime in 2.1-mm borosilicate tube with Parol 70 oil.....	36
Figure 9 Flow regime in 3.7-mm borosilicate glass tube with Parol 70 oil.....	37
Figure 10 Pressure drop in 2.7-mm borosilicate glass with Parol 70 oil .....	38
Figure 11 Pressure drop in 3.7-mm borosilicate glass with Parol 70 oil .....	39
Figure 12 Flow regime in 2.1-mm borosilicate glass tube with Parol 70 and Parol 100 oil.....	43
Figure 13 Flow regime in 3.7-mm borosilicate glass tube with Parol 70 and Parol 100 oil.....	44
Figure 14 3.7 mm borosilicate glass tube flow regime map.....	47
Figure 15 3.7 mm stainless steel tube flow regime map.....	48
Figure 16 4.0 mm Inconel tube flow regime map.....	49
Figure 17 Pressure drop in 3.7-mm stainless steel with Parol 70 oil.....	55
Figure 18 Pressure drop in 4.0-mm Inconel tube with Parol 70 oil.....	56

## List of Tables

Table 1 Liquid-liquid flows in macro-channels.....	6
Table 2 Liquid-liquid flows in micro and mini-channels .....	7
Table 3 Dimensionless numbers used to characterize two-phase flow.....	16
Table 4 Fluid properties .....	26
Table 5 Tube properties and Eötvös number .....	26
Table 6 Flow regime map data for the 2.1-mm borosilicate glass tube with Parol 70 .....	40
Table 7 Flow regime map data for the 3.7-mm borosilicate glass tube with Parol 70 .....	41
Table 8 Flows regime in glass, stainless steel and Inconel at similar oil superficial velocities ( $j_o =$ 0.3 and 0.6 m/s) and same water input ratio .....	53
Table 9 Flow regime in glass, stainless steel and Inconel at similar superficial oil velocities ( $j_o =$ 1.1, 2.2 and 3.4 m/s) and same water input ratio .....	54

## **Acknowledgements**

I would first like to thank my adviser, Dr. Melanie M. Derby, for her patience, motivation, and immense knowledge. I would also like to thank her for taking me under her wing from my junior year of undergrad and helping throughout my time at Kansas State University. I also would like to thank Drs. Eckels and Leseman for making themselves available to me and for their helpful suggestions throughout this work. Special thanks to Jacob Dunshee, G.A. Riley and Michael Brown for their willingness work with me and for their help throughout this work. I would like to thank Dr. Betz and Dr. Wanklyn for always answering my questions or providing me with the resources to find my own answers. I would like to thank the entire CHIL lab for being part of my journey, Jordan, Ryan, Nicole and especially Chen for his wise suggestions and his family for the home cooked meals. I would also like to thank Eric Wagner and James Hodgson for helping me find my way around a machine shop. I would like to give a big shoutout to Brandon Reid for challenging me to be the best version of myself in all phases of life. I have deep gratitude to many of my friends who continuously encouraged me not to doubt myself and to always think positively, Minh, Edgar, Asrar, Zayed, Jignesh, Monsur, Long, Hai, Geordy, Carrington and many others.

Special thanks to my beautiful fiancée Lilia Flores for her unconditional love and her genuine care for my wellbeing in all phases of life. Finally I would like to thank The Bultongez family, starting with my parents, Dream and Chantal, my older and younger sister, Amanda and Joyce, respectively and my three younger brothers, Ronald, Elton and Beni. I owe a special thanks to my man Jesse Bultongez, there isn't enough words to show how thankful I am such a powerful relationship.

I would also like to thank Dr. Diana Grauer for her guidance and OneSubsea for funding the project. This work would not be possible without the help of our sponsor.

# Chapter 1 - INTRODUCTION

## 1.1 Motivation

Petroleum is the largest primary energy source in the U.S. accounting for 36% of the overall energy consumed. Oil-based energy fuels makes up 92% of the entire transportation sector and 39% of the industrial sector [1]. According to the Energy Information Administration, oil-derived fuel sources will continue to be integral in supplying energy to the U.S. in the coming decades. Technological advancements have led to an increase in deepwater and ultra deepwater exploration. Offshore oil production in the U.S. has increased by 6.5% from 2005 to 2015 [2]. In 2009, 45% of new oil discoveries were in deepwater and ultra deep water regions at water depths greater than 400 m [3]. Oil production processes done on ships and land have shown to be more difficult to accomplish in subsea applications. The challenges of working at these water depths have proven to be significant, as demonstrated by recent oil spills into the Gulf of Mexico.

Desalting, the removal of salt water from crude oil, is a process carried out systematically to reduce pipe corrosion and to prolong equipment life and is among the various processes that increase in difficulty at deepwater and ultra deepwater depths. Present desalting technologies utilize gravitational and electrostatic forces to remove salt water from crude oil. In the case of heavy crude oil, with oil densities approaching that of water, gravitational forces alone are insufficient in separating salt water from crude oil. Electrostatic forces enhance gravitational separation processes by means of electrostatic coalescence of water droplets. However, electrostatic separation typically require voltages in excess of 30,000 V [4], a challenging load to supply to the ocean floor in subsea applications since desalting is typically done close the well head. Initializing oil and water separation within the pipe before reaching the desalting equipment in a passive manner could be a

potential solution to the current desalting challenges and a valuable addition to current oil-water separation technologies.

Surface tension forces provide potential and is a promising new approach to address these challenges. Surface tension impacts on flow regime have been detected even at low oil-water density differences and are stronger as tube size decreases [5]. Liquid-liquid surface tension driven flows in mini-channels have been documented to display particular sets and ranges of flow configurations (i.e. annular flow) [6]. Annular flow is a desirable flow regime in terms of pressure gradient and provides numerous potential implementations of surface-tension driven flow for passive oil-water separation. Annular flow, salt water surrounding an oil core, combined with a porous membrane in a honey-comb pattern where water could be extracted and directed to water-only pipes could be a possible approach to utilizing surface-tension annular flow. Increase understanding of oil-water flow patterns and pressure gradient in mini-channels can offer insight on utilizing surface tension forces for desalting systems.

## Chapter 2 - LITERATURE REVIEW

### 2.1 Background

Multiphase flows are prevalent in the oil industry. The classification of two phase flows in the petroleum industry includes gas-solid flows, gas-liquid flows, liquid-liquid flows and liquid-solid flows. The nuclear industry, having special interest in steam-water flows for cooling systems, has been the driving force in the extensive investigation of gas-liquid flows and has facilitated the advancement and understanding of two-phase flow regime and pressure drop prediction models [7]. Compared to gas-liquid flows, liquid-liquid flows have received less attention and represent an area of further fundamental research.

Despite the comprehensive data available with gas-liquid flows, holdup, flow regime and pressure gradient prediction models are not readily interchangeable with liquid-liquid flows. One of the biggest reasons is that gas-liquid flow density ratios are significantly different than liquid-liquid flows. Gas-liquid flow densities can differ by three orders of magnitude [6-8] while density differences are much lower in oil-water, especially in the case of heavy crude oil where densities approach that of water [5, 8, 9]. Similarly, single-phase liquid flow models cannot be used in multiphase liquid-liquid flows mainly due to wall and interfacial shear stresses. In oil-water flows, shear stresses can be up to four times that of single-phase stresses [5]. Russel et al. [10] and Charles et al. [11] were some of the first researchers to investigate liquid-liquid flow in the late 1950s and early 1960s, respectively. They specifically observed oil-water flows with hopes to reduce pressure drops in oil extraction processes. The need to enhance flow regime and pressure drop prediction models along with holdup led to a new found interest in liquid-liquid flows around the 1990s [7, 12].

## **2.2 Oil-water flow regimes**

Oil-water flows in horizontal tubes display a variety of flow regimes that depend on fluid properties, tube size, along with flow conditions (i.e. phase fraction, water and oil velocities) [6, 13]. Bannwart et al. [13] and other authors [6, 9, 12-31] categorized oil-water flow regimes using a gas-liquid analogy. The liquid-liquid flow regimes can be divided into three major categories: separated flow, intermittent flow and dispersed flow.

The separated flow regime category consists of flow patterns that show continuity in both phases and distinct separation between the oil and water phase [32]. Stratified and annular flow are two main types of separated flows that have consistently been documented. These separated flow have sub flow descriptions (e.g. wavy, churn, dispersed etc.) and are highly dependent on tube size in addition to fluid velocities and phase fraction. A wide range of oil-water flow regime can be classified under the intermittent flow regime category. All separated flows that are no longer continuous in nature become intermittent. Intermittent flows have been observed over all tube sizes and are mainly dependent on fluid velocities and contain flows such as: slug flow, plug flow, irregular flow and droplet flow [9-14, 17, 22, 26, 29-31, 33-39]. The dispersed flow regime is also majorly dependent on fluid velocities and it consists of one phase in droplet form, large or fine in size, scattered throughout the other phase [18, 19]. Similar to intermittent flow, dispersed flow has been observed and investigated over a wide range of oil-water flow conditions.

## **2.3 Effects of channel size on flow regimes**

Oil-water flows in horizontal tubes have been studied in a variety of tube sizes. Table 1 and Table 2 and provide a list of studied liquid-liquid flow patterns, mostly oil-water, in horizontal tubes of different sizes, materials and different oil densities and viscosities. Brauner et al. [6]

classified liquid-liquid flow regimes based on the non-dimensional Eötvös number, which is defined as the ratio between gravitational and surface tension forces:  $Eo_D = \frac{\Delta\rho g D^2}{8\sigma}$  where  $D$  and  $g$  are the tube diameter and gravitational acceleration, respectively,  $\Delta\rho$  is the difference in densities between the liquids and  $\sigma$  is the surface tension between the two liquids [6, 32, 40].

Larger Eötvös numbers (i.e.,  $Eo_D > 1$ ) Table 1, correlate to dominant gravitational forces and are associated with macro-channels. The dominant gravitational forces in macro-channels generate a wider range of stratified regimes at relatively liquid low flow rates [5, 12, 14, 17, 21-24, 27, 28]. Interfacial waves have been observed by many researchers in stratified flow [14, 15, 21, 23, 27]; this stratified-wavy flow pattern indicates instabilities stemming from different oil and water flow velocities. These interfacial waves increased droplet entrainment (e.g., oil droplets in water or water droplets in oil), thereby transitioning to dispersed flow regimes [16, 18, 19, 26, 27, 41, 42]. Dispersed flow is prevalent at high flow velocities and observed to have a wider range in macro-channels.

At small Eötvös numbers (i.e.,  $Eo_D < 1$ ) found in micro and mini-channels, corresponds to dominant surface tension forces. Liquid-liquid flows in micro and mini-channels, shown in Table 1, have received a lot of attention in chemical processes such as nitration, polymerization, phase transfer catalysis, reactive extraction, solvent extraction [37, 43], with specific interest in slug flow while mini-channels have not been investigated to the same extent. In micro and mini-channels, the natural tendency for gravity to create stratification of the different fluid densities between oil-water is offset by the increasing influence of surface tension forces, allowing annular flow, plug flow, slug flow to occur over a wider range [29, 34, 36, 37].

**Table 1 Liquid-liquid flows in macro-channels**

System	Tube size and material	Fluid properties, $\sigma$ (mN/m)	Flow regimes
Kerosene - water Mandal et al. [9]	D= 12, 25 mm; PMMA	$\mu_1/\mu_2=1.2$ ; $\rho_1/\rho_2=0.787$ ;	stratified, plug, slug, three-layer, rivulet, churn dispersed flow
Lubricating oil - water Kerosene - water Balakhrisna et al. [38]	D= 12, 25.4 mm; acrylic resin	$\mu_1/\mu_2=200, 1.2$ ; $\rho_1/\rho_2=0.960,$ $0.787$ ; $\sigma = 55, 36$	core, plug, dispersed flow
Kerosene- perchloroethylene - water Hasson et al. [39]	D= 12.6 mm; glass	$\mu_1/\mu_2=1.22;$ $\rho_1/\rho_2=1.02$ ; $\sigma = 17.3$	stratified, slug, annular, dispersed flow
Oil - water Al-Wahabi et al. [14]	D= 14 mm; acrylic	$\mu_1/\mu_2=5.5$ ; $\rho_1/\rho_2=0.828$ ; $\sigma = 39.6$	stratified, annular, slug, bubbly, dual continuous flow
Oil - water Angeli et al. [22]	D= 14 mm; acrylic	$\mu_1/\mu_2=5.5$ ; $\rho_1/\rho_2=0.828$ ; $\sigma = 39.6$	stratified, rivulet, dispersed flow
Oil - water Russell et al. [10]	D= 20.3 mm; cellulose acetate- butyrate	$\mu_1/\mu_2=20.13$ ; $\rho_1/\rho_2=0.84$ ;	stratified, concentric, dispersed flow
Oil - water Charles et al. [11]	D= 26 mm; cellulose acetate- butyrate	$\mu_1/\mu_2=6.29, 16.8,$ $65$ ; $\rho_1/\rho_2=0.998$ ; $\sigma = 44, 45, 30$	drops, concentric, slugs, bubbles flow
Crude oil - water Bannwart et al. [12]	D= 28.4 mm; PVC	$\mu_1/\mu_2= 488$ ; $\rho_1/\rho_2= 0.925$ ; $\sigma = 29$	stratified, bubbles, annular, dispersed flow
Crude oil - water Bannwart et al. [13]	D= 28.4 mm; glass	$\mu_1/\mu_2=3400$ ; $\rho_1/\rho_2=0.97$ ;	stratified, bubbles, annular, intermittent flow
Mineral oil - water Atmaca et al. [17]	D= 50.8 mm; PVC	$\mu_1/\mu_2=13.5$ ; $\rho_1/\rho_2=0.859$ ; $\sigma = 16.38$ mN/m	stratified, dispersed flow

**Table 2 Liquid-liquid flows in micro and mini-channels**

System	Tube size and material	Fluid properties, $\sigma$ (mN/m)	Flow regimes
Acetone-toluene - water Kashid et al. [33]	D= 150, 269, 400, 500 $\mu\text{m}$ ; glass	$\mu_1/\mu_2=0.59$ ;	slug, annular, intermittent, dispersed flow
Ionic liquid - water Tsaoulidis et al. [30]	D= 200 $\mu\text{m}$ ; glass D=220 $\mu\text{m}$ ; FEP D= 270 $\mu\text{m}$ ; Tefzel	$\mu_1/\mu_2=41$ ; $\rho_1/\rho_2=1.42$ ; $\sigma = 12.3$	plug, intermittent, annular, drop, dispersed, irregular flow
Ethylene glycol - water Jovanovic'et al. [34]	D= 248 and 498 $\mu\text{m}$	$\mu_1/\mu_2=2.46$ ; $\rho_1/\rho_2=1.04$ ; $\sigma = 30$	slug flow
Kerosene - water Zhao et al. [31]	D= 400 $\mu\text{m}$ ; PMMA	$\mu_1/\mu_2=1.15$ ; $\rho_1/\rho_2=0.781$ ; $\sigma = 45$	slug, dispersed, parallel flow
Mineral oil - water Salim et al. [25]	D= 793 $\mu\text{m}$ ; quartz D=667 $\mu\text{m}$ ; glass	$\mu_1/\mu_2=31$ ; $\rho_1/\rho_2=0.843$ ; $\sigma = 30.1$	droplet, slug, annular, parallel flow
Ionic liquid - $\text{HNO}_3$ Tsaoulidis et al. [29]	D= 0.5, 1, and 2 mm ; Teflon	$\mu_1/\mu_2=52$ ; $\rho_1/\rho_2=1.42$ ; $\sigma = 10.0$	plug flow
Hexadecane - water Fletcher et al. [36]	D= 1.06 mm; stainless steel	$\mu_1/\mu_2=0.337$ ; $\rho_1/\rho_2=0.772$ ; $\sigma = 51.1$	slug flow
Toluene - water Das et al. [37]	D= 2 mm and 6 mm; glass	$\rho_1/\rho_2=0.85$ ; $\sigma = 30.1$	stratified, annular, plug flow

## 2.4 Flow regime transitions

### 2.4.1 Macro-channels

Macro-channels have been the primary subject of flow patterns and transition studies predominantly consist of macro-channels with diameter  $D_H > 10$  mm [31]. Horizontal oil-water flows in large tube diameters (i.e.,  $Eo_D > 1$ ) typically present the ideal environment for stratified flow. Stratified flow without entrainment (i.e., complete separation) exists at relatively low flow rates where, due to the density difference, the dominant gravitational forces greatly stabilize the flow, producing a smooth oil-water interface. Increasing flow velocities induces interfacial waves between the two phases. As flow rates continue to increase, droplets begin to form, marking the onset of entrainment. The transition from stratified to dispersed flow occurs at high water flow rates where the oil phase is no longer continuous, resulting in an oil-in-water dispersion and eventually to an emulsion flow [17, 44]. At higher oil viscosities, stratified flow transitions to intermittent slug, plug, or bubble flow before reaching dispersed flow as velocities continue to increase [12, 13, 26]. Under certain conditions, stratified flow was observed to transition to annular flow in macro-channels [10, 11, 14, 38, 39]. However, these annular flow regimes were only observed for small ranges. Annular flow requires relatively high oil flow rates to sufficiently stabilize. These same high flow conditions and low oil viscosity expedite the process of entrainment causing a destruction of the annular phase and shorting its range of existence [6].

### 2.4.2 Micro- and mini-channels

In recent years, the interest in microfluidic technology has greatly risen, as it offers new prospects for emulsion science and allowed for the development of lab-on-a-chip technologies which has revolutionized analytical laboratories and created platforms for personalized diagnostics

and high-throughput drug discovery [45, 46]. The main oil-water flows observed in micro and mini-channels consist of annular flow, slug and plug flow of the wetting phase and dispersed flow. Stratified flow cannot be attained in micro-channel flows and only span a small range of mini-channels [6, 32], even at low oil densities and flow conditions. Liquid-liquid flows in micro and mini-channels (i.e.,  $E_{OD} \ll 1$ ) are different than macro-channels in that surface tension forces have significantly stronger effects on flow regime.

Annular flow is a highly desired flow regime. The water annulus serves as a lubricant to the oil core which greatly reduces pressure loss increasing power savings when transporting viscous liquids (e.g. heavy crude oil) and it exists at wider range of flow conditions in micro and mini-channels [6, 7, 32, 39]. The hydrodynamic instabilities in annular flow result in a wavy oil-water interface. The development of a wavy core interface is believed to be essential in the stabilization of annular [32]. However, the increase in interfacial waves under higher flow conditions facilitates the droplet entrainment and the transition to dispersed flow. Oliemans et al. [47] concluded that, the smaller the annulus thickness at the wall the stronger the reducing effect on the growth of Rayleigh-Taylor and Kelvin-Helmholtz instabilities at the interface between the two liquids.

## **2.5 Effects of tube properties on oil-water flows**

In macro-channels, surface tension and capillary forces are negligible in comparison to inertial and viscous forces. However, as tube diameters decrease (i.e.,  $E_{OD} \ll 1$ ) capillary effects begin to play an important role in altering oil-water flow regime [48]. In micro and mini-channels, wettability of the liquids with the tube wall have significant effect on flow regime. For this reason, given the same operational conditions, different flow patterns may result by changing the tube

material [6]. Tsaoulidis et al. [30] investigated flow in glass, FEP and Tefzel with tube diameter of 200  $\mu\text{m}$ , 220  $\mu\text{m}$ , 270  $\mu\text{m}$  respectively. Wettability was an important factor that contributed in flow regime. The glass had a recorded contact angle of  $55^\circ$  while both Teflon tube, FEP and Tefzel, having contact angles of  $102^\circ$ . The authors observed that flow in the glass tube were highly effected by the fluid that first wetted the channel. In all flow regimes, water was always the continuous phase and in full contact with the glass tube walls. The main flow observed in the glass tube were plug flow and intermittent flow. The Teflon tubes behaved similarly to one another, however, they were different than the glass tube. The main flow observed in the Teflon tubes were annular flow, with water flowing in the core, plug flow and drop flow, with water being the encapsulated liquid. Brauner et al. elaborates on this phenomena occurring in the hydrophobic tubes and call it inverted annular flow [32]. Where oil flows in the annulus and water in the core due to the hydrophobic nature of the tube wall. This is something that has not been observed or documented in larger tube sizes.

## **2.6 Conclusions from literature review**

From the literature review, the following conclusion can be drawn:

- Two phase liquid-liquid research has not received the same attention as gas-liquid flows over the years. The comprehensive data base of flow regime and pressure drop models available for single-phase and two-phase gas-liquid flows cannot readily be used for liquid-liquid systems. Compared to two-phase gas-liquid flows under similar flow conditions, liquid-liquid flows behave differently due to difference in fluid density and viscosity ratios [5, 8, 9]. In the case of single-phase, shear forces in two-phase liquid-liquid can be up to 400% higher at similar flow velocity [5].

- Oil-water flow in horizontal tubes are dependent on oil and water fluid properties as well as tube properties (e.g. tube size and wettability). Oil-water flow research has placed more attention in larger size tubes for oil extraction and transportation over the years. Liquid-liquid flow in micro- and mini-channels need more attention, especially in mini-channels as the gravitational are still present while capillary surface tension forces become significant in controlling flow regime.
- Oil-water flow regimes typically observed in horizontal macro-channel tubes consist of: stratified flow, intermittent and dispersed flow. Intermittent flow includes: slug, plug, droplet and irregular. Stratified flow, a gravity dominant flow, is not observed in micro-channels and spans a small range in mini-channels [10, 11, 14, 38, 39].
- Annular flow is a popular flow in the petroleum industry, due to pressure reduction capabilities, and spans a much wider range in micro and mini-tubes. While tube material properties (e.g. wettability) do not have much of an effect in large macro-channels, it hold importance in micro and mini-channels. Hydrophobic tube material displayed inverted flow regimes, where water acted as the core annulus and the slug or plug in micro-channels [30, 32].

## **2.7 Research objectives**

Effects of capillary surface tension forces and small tube diameter size have significant effects on oil-water flow regime. The literature review demonstrated the lack of documentation on oil-water flow in micro and mini-channels. The literature is especially limited in mini-channel oil-water flow as mini-channels range across the boundary where gravitational begin to diminish and surface tension critically influential in flow regimes.

The ultimate aspiration of this project is utilize the annular flow regime to build passive oil-water separation device for desalting processes in deep sea drilling application. Expanding and solidifying understanding in mini-scale oil-water flow regimes and pressure drops is an initial step towards developing a surface-tension-driven oil-water separation system.

In taking the first steps, the objectives of this research are to investigate the effects of mini-tube diameter, oil viscosity, and tube material on flow regime and pressure drop mini-channel oil-water flows. This was done by investigating a 2.1-mm and 3.7-mm borosilicate glass tube, a 3.7-mm stainless steel tube and a 4-mm Inconel tube using two mineral oils of equal density with viscosity ratio of two.

## **Chapter 3 - EXPERIMENTAL DESIGN**

### **3.1 Experimental apparatus design**

An adiabatic closed loop experimental apparatus, shown in, Figure 1 was constructed to study and accurately measure liquid-liquid two-phase flow regimes and pressure drop. Water and mineral oil (Parol ® 70 or Parol ® 100, Calumet) were tested for a range of oil and water velocities. Fluid properties are listed in Table 4. The addition of salt to water is known to increase surface tension while barely altering its specific gravity [49], therefore tap water was selected instead of salt water to conduct this study in the interest of convenience and life of all components. The closed loop apparatus begins and ends with a 30-gallon pressure vessel where both fluids (i.e., oil and water) are stored and separated via gravity. The fluids were pumped separately from the storage tank and through the experimental apparatus via two external gear pumps controlled by their respective variable frequency drives. Oil and water mass flow rates were adjusted and regulated through a series of valves, in addition to the variable frequency drives. The two streams then entered their respective Coriolis flow meters where mass flow rate, density and temperature of each fluid were measured and recorded. Upon passing through their respective Coriolis flow meters, the fluids were then mixed together in a Y-junction before entering the test section. Inlet and outlet pressure and temperature measurements were collected to confirm adiabatic conditions throughout data collection.

### **3.2 Test section design**

The test section was designed to accurately measure pressure drop and visualize two-phase flow regimes. The test section, shown in Figure 2, consisted of two main regions, the developing region (A) and the fully developed region (B) with the addition of a sight glass for the metallic

tubes tested. Lengths (A) and (B) varied across the tubes tested as follows: 2.1-mm borosilicate glass tube, A=0.464-m and B=0.322-m; 3.7-mm borosilicate glass tube, A=0.735-m and B=0.495-m; the stainless steel and Inconel tubes both had the same dimensions at A=0.725 and B=0.387-m. A Teflon insert, matching the diameter inside diameter, was used inside the tee fitting connecting the developing region and the fully developed region of the test section to maintain flow regime through the tee fitting tube expansion. A differential pressure transducer measured two-phase flow pressure drops across the fully developed region. Flow regimes were visualized through the fully developed region for the borosilicate glass tube and through a sight glass for both stainless steel and Inconel tubes using a microscope (Leica S6 D) and high-speed camera (Fastec IL5). Green food coloring, only immiscible in water, was used in order to enhance oil-water interface flow.

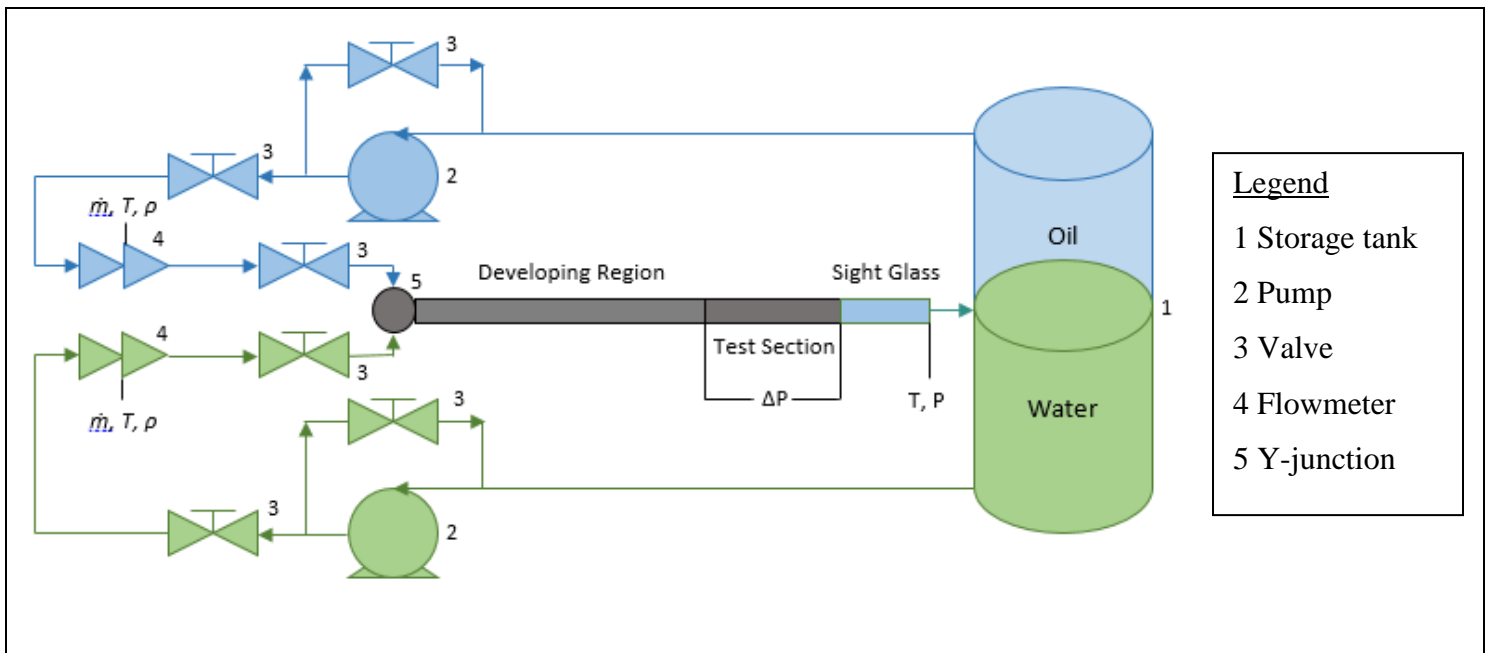


**Figure 1 Experimental apparatus for mini-channel oil and water flows**

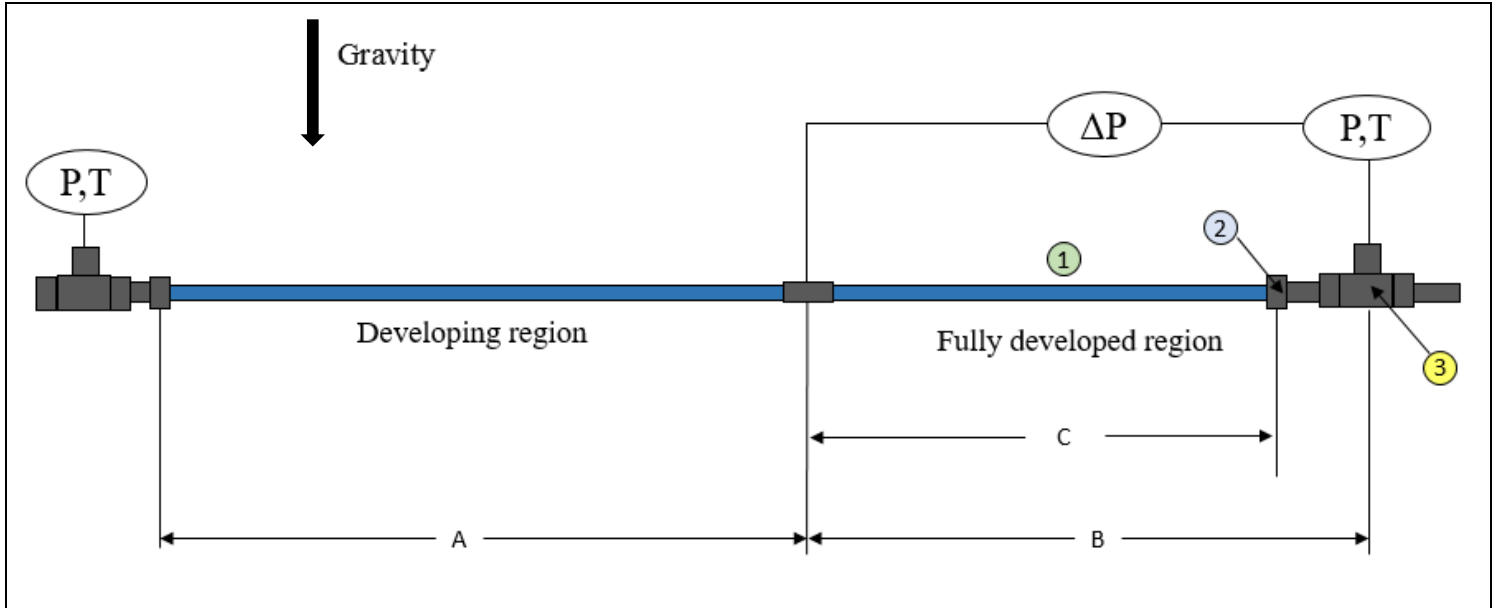


**Figure 2 Test section**

### 3.3 Governing parameters

Interactions between inertial, viscous, gravitational, and surface tension forces influence flow regimes in two-phase flows. Fluid velocities, phase holdup, fluid properties, channel material and geometry are all factors that impact flow regimes and pressure drops. These forces are typically quantified in the form of dimensionless numbers such as Capillary, Eötvös and Reynolds numbers. The Capillary number relates the relationship between viscous and interfacial forces. The Reynolds number relates inertial to viscous forces and the relationship between gravitational and surface tension forces is described by the Eötvös number. The Eötvös and Reynolds numbers, shown in Table 3, are calculated based on the characteristic length of mini-channel diameter in this study, whereas characteristic length is not necessary for the Capillary number.

The Capillary number is calculated using the mixture superficial velocity and viscosity. In complex two-phase flows, actual fluid velocity is often spatially dependent and subject to many assumptions, making it very challenging to measure. Instead, superficial velocity is used because

it can be calculated with readily known parameters. The superficial velocity is defined as the volumetric flow rate of a fluid flowing in a pipe divided by the pipe's cross-sectional area,

$$j_w = \frac{\dot{m}_w}{\rho_w A}; \quad j_o = \frac{\dot{m}_o}{\rho_o A} \quad \text{Eq. (1)}$$

where  $j_w, j_o, \dot{m}_w, \dot{m}_o, \rho_w, \rho_o$  and  $A$  are the superficial velocities, mass flow rates, densities and cross-sectional area for water and oil, respectively. For the purposes of the Capillary number, the mixture viscosity is defined using a weighted mass average using mass flow rate,

$$\mu_{ow} = \left( \frac{\dot{m}_w}{\dot{m}_w + \dot{m}_o} \right) \mu_w + \left( \frac{\dot{m}_o}{\dot{m}_w + \dot{m}_o} \right) \mu_o \quad \text{Eq. (2)}$$

where the subscript  $ow$  stands for oil-water mixture. Forces are balanced at Capillary and Eötvös number close to 1. Brauner and Moalem-Maron et al. [6] used the non-dimensional Eötvös number to characterize the surface tension dominance in two-phase flow in micro and mini-channels. The Reynolds is calculated using the mass flow rates and properties of each individual phases as shown in Table 3.

**Table 3 Dimensionless numbers used to characterize two-phase flow**

Dimensionless number	Definition
Capillary number	$Ca_{ow} = \frac{\mu_{ow} j_{ow}}{\sigma}$
Eötvös number	$EO_D = \frac{\Delta \rho g D^2}{\sigma}$
Reynolds number	$Re_i = \frac{4 \dot{m}_i}{\pi D \mu_i}$

### 3.4 Instrumentation

The experimental apparatus was designed to provide a wide range of experimental conditions. To acquire identification and measurements of all needed flow parameters, various instruments were used (Figure 2).

#### Separation tank

The separation tank consisted of an ASME 30-gallon 316L stainless steel pressure vessel with an overall height of about 33-in and 18-in wide with two 1/2 inch and one 3/8 inch accessible port. Two ports were used as oil and water outlets and were connected to their respective pumps via flexible stainless steel tubing. The third port was connected to the test section outlet and was used as the return port, thereby closing the experimental apparatus loop. The separation tank was filled with 20-gallon of oil and 10 gallons of water. Oil and water mixtures were returned about half way of the height of the tank and were separated via gravity, forming an emulsion layer inside the tank. Oil was tapped from the top while water was retrieved from the bottom of the tank to avoid pumping the mixed fluid. Density measurements were taken continuously with the Coriolis flow meters to validate that 100% oil or water were being pumped through respective pumps before entering the test section.

#### Pumps

Two external gear pumpheads (GC-M25. PF5S.E) assembled with two 1-HP 3450-RPM 3-phase 60 Hz TEFC electric motors (CEM3545 Baldor, Burt Processes) were used to pump each fluid. Two variable frequency drives (ACS250-01U-04-13-1 IP20, Burt Processes) with 0–60 Hz control frequency with 110–120 V supply and 200–240 V 3-phase output were used to control the pump motors, enabling flow rate control.

#### Flowmeters

Two Coriolis flow meter (CMFS015M, Micro Motion) were used to collect mass flow rate, density, and temperature measurements with accuracies of  $\pm 0.05\%$  of mass flow rate,  $\pm 0.2 \text{ kg/m}^3$  of reading, and  $\pm 0.2 \text{ }^\circ\text{C}$  of reading, respectively. The data were collected for each fluid separately before mixing and entering the test section. Oil and water mass flow measurements with relatively high accuracy were necessary for calculations of water input ratio and oil-water superficial velocities, respectively.

### Pressure

Two gage pressure transducers (PX303-200G5V, Omega), of range 0-200 PSI with accuracies of  $\pm 0.25\%$  full scale, were used to measure the inlet and outlet pressures of the entire test section. High output low differential bidirectional pressure transducer designed for wet-to-wet differential pressure measurements (Model 230, Setra) with a range of 0–5-PSI and 0–50-PSI and accuracy of  $\pm 0.25\%$  full scale were used to measure the differential pressure in the fully developed region of the test section. All pressure transducers were calibrated using a ball-type deadweight tester with accuracy range of 0–300 psi and accuracy of  $\pm 0.015\%$  of reading.

### Temperature

Type T thermocouples (TMQSS-062U, Omega) made with special limits of error thermocouple material were calibrated against a reference thermometer (Omega HH41) with accuracy of  $\pm 0.05 \text{ }^\circ\text{C}$  in a water bath at ten temperature points over a temperature range and including ice and boiling points. Thermocouple calibration resulted in an uncertainty of  $\pm 0.2 \text{ }^\circ\text{C}$ . Temperature measurements were taken at the inlet and exit of the test section to ensure adiabatic conditions and were logged continuously throughout the experimental data collection.

### 3.5 Experimental procedures

In order to validate the experimental apparatus, single-phase water tests were conducted. For these experiments, a range of water mass flowrates ( $\dot{m}_w$ ) were selected and tested. Pressure, temperature, and density measurements were taken at each water mass flowrate ( $\dot{m}_w$ ) and compared to predicted values. Single-phase tests results showed excellent agreement with the experimental results yielding a mean percent error below 5% for both tube materials. The apparatus was validated with single phase flow before proceeding to two-phase data collection, see page 20 for details. The different flow regimes analyzed in this study were obtained by controlling the oil and water mass flow rates. The experimental oil and water flow data are presented in terms of superficial velocity and water input ratio. The water input ratio,  $\varepsilon$ , defined as the ratio between the water superficial velocity and the mean velocity of the two phases along water mass flow rate [41], was selected as a controlling variable to investigate the effects of different water flow rates on flow regimes,

$$\varepsilon = \frac{j_w}{j_o + j_w} = \frac{\dot{m}_w}{\frac{\rho_w \dot{m}_o}{\rho_o} + \dot{m}_w}; \dot{m}_w = \frac{\varepsilon \rho_w \dot{m}_o}{(1 - \varepsilon) \rho_o} \quad \text{Eq. (3)}$$

The following procedure was used to collect the experimental two-phase data: The following procedure was used to collect the experimental two-phase data:

1. An oil mass flowrate ( $\dot{m}_o$ ) was selected along with a minimum and maximum water input ratio ( $\varepsilon$ ).
2. The water mass flowrate ( $\dot{m}_w$ ) for each water input ratio ( $\varepsilon$ ) was calculated, beginning at the minimum water input ratio ( $\varepsilon_{min}$ ) and increasing by ten percent until the maximum water input ratio ( $\varepsilon_{max}$ ) was reached.
3. Oil and water were introduced into the test section.

4. The oil was set to the selected oil mass flowrate ( $\dot{m}_o$ ). The water was set to the water mass flowrate ( $\dot{m}_w$ ) corresponding to the minimum water input ratio ( $\epsilon_{min}$ ).
5. Once steady state was achieved, the pressure, temperature, density, and flowrate measurements were collected. Flow visualization was also done at this time.
6. The water mass flowrate ( $\dot{m}_w$ ) was increased to reach the next water input ratio ( $\epsilon$ ), and the oil mass flowrate ( $\dot{m}_o$ ) was adjusted to remain fixed.
7. Steps 6 and 7 were repeated until data collection and flow visualization occurred at the maximum water input ratio ( $\epsilon_{max}$ ).
8. Steps 1 through 8 were repeated at a new oil mass flowrate ( $\dot{m}_o$ ).

### 3.6 Single-phase validation

Single-phase tests were conducted using tap water to validate the experimental apparatus instrumentation. The total pressure drop in the test section was modeled to predict the pressure drop across the fully developed region of the test section. The model accounted for the minor losses in the diameter expansions between the glass tube and tube adapter (i.e., component (1-2)) and tube adapter to cross fitting (i.e., component (2-3)). The Darcy-Weisbach equation for pressure frictional loss along with the minor losses equation was used to calculate the pressure drop in the fully developed region of the test section, with the objective to confirm that minor losses across the measured length were negligible. Total pressure drop was modeled as

$$P_{total} = \Sigma\Delta P_{major} + \Sigma\Delta P_{minor} \quad \text{Eq. (4)}$$

$$\Delta P_{major} = \frac{8fL\dot{m}^2}{\rho\pi^2D^5} \quad \text{Eq. (5)}$$

$$\Delta P_{\text{minor}} = \frac{8K\dot{m}^2}{\rho\pi^2D^5} \quad \text{Eq. (6)}$$

where  $\Delta P_{\text{total}}$  is the total pressure drop across all three components consisting of major and minor losses,  $\Delta P_{\text{major}}$  and  $\Delta P_{\text{minor}}$  are the sum of all major and minor losses, respectively.  $L$ ,  $D$ ,  $\dot{m}$  and  $\rho$ , represent the length of the glass tube (component (1)), tube diameter, water mass flow rate, and water density, respectively, and  $f$  and  $K$  are the Darcy's friction factor and minor loss coefficients, respectively. The minor head loss equation was used to calculate the pressure drop in the diameter expansions between components using minor loss coefficients of  $K_1 = 0.6$  and  $K_2 = 0.23$ , for the diameter expansions between component (1-2) and (2-3),[50]. The Colebrook-Haaland equation was used to calculate the friction factor for turbulent water flows in the 465-mm long glass and the tube adaptor, components (1) and (2) respectively,

$$f = \frac{64}{Re} \quad \text{Eq. (7)}$$

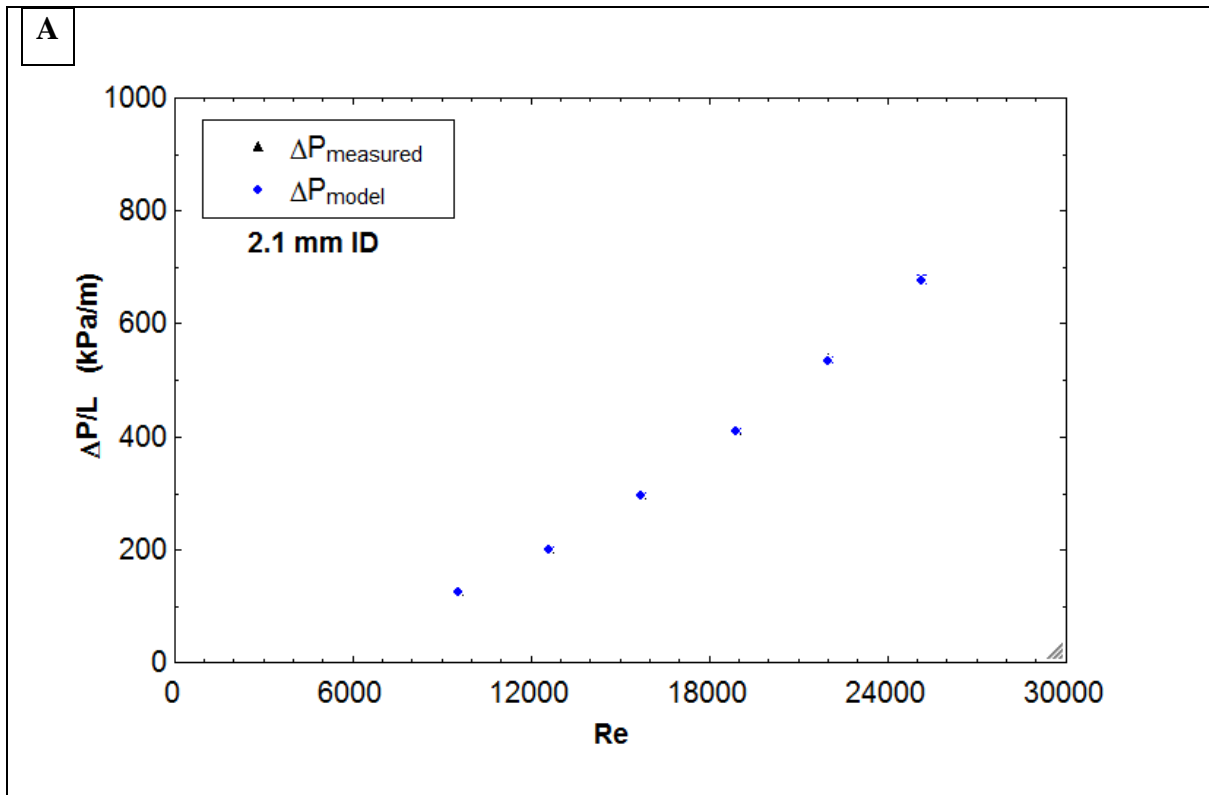
$$\frac{1}{\sqrt{f}} = -1.8 \log_{10} \left[ \left( \frac{e/D}{3.7} \right)^{1.11} + \frac{6.9}{Re} \right] \quad Re > 4000 \quad \text{Eq. (8)}$$

$$Re = \frac{4 \dot{m}}{\pi\mu D} \quad \text{Eq. (9)}$$

where  $Re$  is Reynolds number,  $\mu$  is viscosity and  $e/D$  represents the relative tube roughness. The glass tube was modeled as a smooth pipe and a standard absolute roughness of  $e = 1.5E-5$  m was used for the stainless steel tube adapter and component (2).

The water temperature of 22 °C and subsequent density of 998 kg/m<sup>3</sup> were maintained throughout the entire experiment. A 5-psi and 50-psi pressure transducer (Setra) with  $\pm 0.25\%$  FS accuracy were used in the 3.7-mm and 2.1-mm tubes, respectively, for single-phase validation tests. Figure 3 displays the results obtained from the pressure drop model compared to the

measured data. The analytical pressure drop model showed excellent agreement with the experimental results with a mean percent error of under 5% for both diameter tubes. Single-phase tests results indicate that the vast majority (98 %) of measured pressure drop was found in the glass portion of test section, Figure 2, component (1), resulting in negligible minor losses. Therefore, measured oil-water pressure drops will accurately represent two-phase pressure drops.



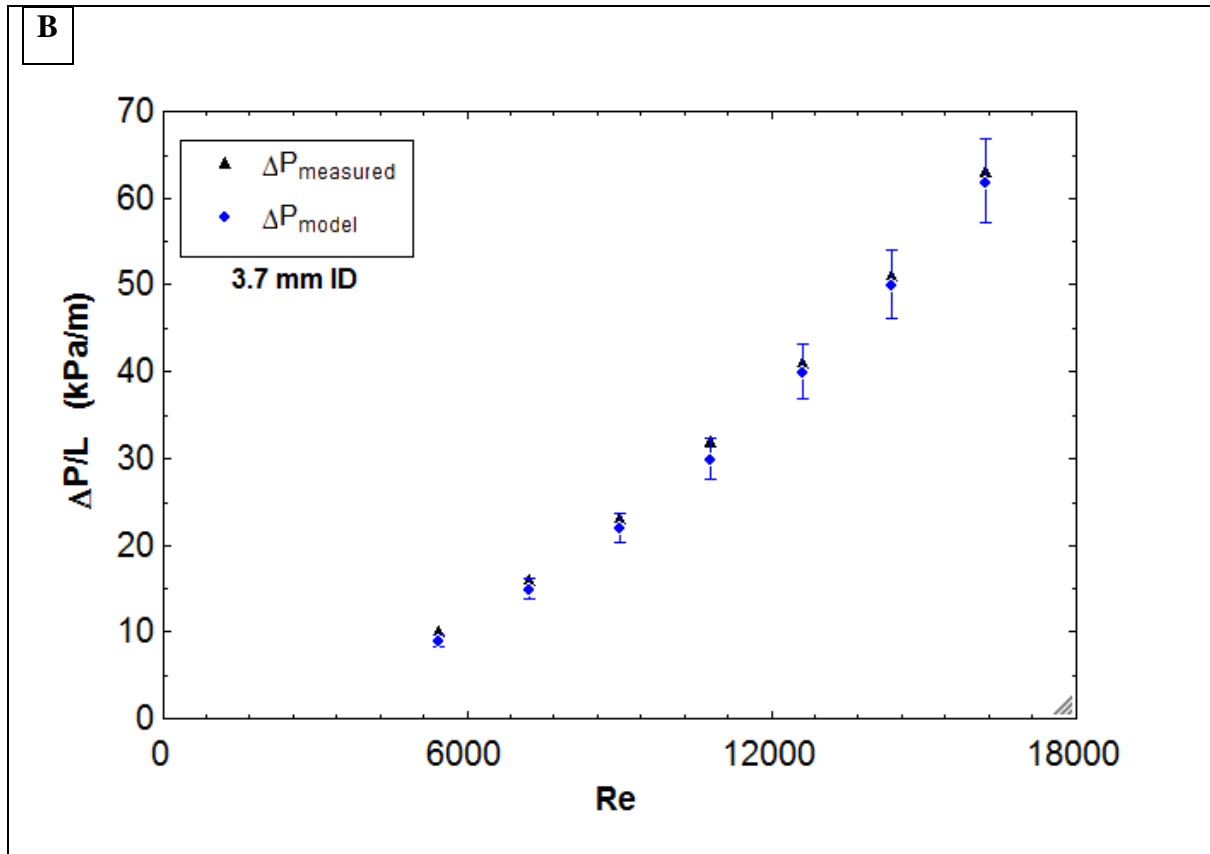


Figure 3 Single-phase water pressure drop on borosilicate glass tube A) 2.1 mm B) 3.7 mm

### 3.7 Uncertainty analysis

A propagation of uncertainty analysis was conducted in order to determine the total uncertainty in the test section differential pressure measurements. The differential pressure drop was a function of tube length and diameter, friction factor, mass flow rate and fluid density, Eq. (5). Each variable's uncertainty was taken into consideration in order to validate the single-phase experimental pressure drop. Uncertainties in tube length, mass flow rate and fluid density were taken directly from respective measuring device accuracy. The working tube diameter was found by inserting a precise known volume of water into a measured tube length and calculated with the following equation

$$D = \sqrt{\frac{4V}{\pi h}} \quad \text{Eq. (10)}$$

where  $D$  is the working tube diameter,  $V$  and  $h$  are the volume and tube height, respectively. Tube volume and heights measurements were taken for a dozen of tubes varying in lengths to decrease personal errors. The uncertainty in the tube diameter was then

$$w_D = \sqrt{\left(\frac{\partial D}{\partial V} \frac{V}{D} w_V\right)^2 + \left(\frac{\partial D}{\partial h} \frac{h}{D} w_h\right)^2} \quad \text{Eq. (11)}$$

Where  $w_D$  is the propagated uncertainty for the tube diameter,  $w_V$  and  $w_h$  are the volume and height measurement uncertainties. Maximum uncertainties of  $w_V$  and  $w_h$  were  $\pm 2\%$  and  $\pm 0.7\%$ , respectively. The total propagated uncertainty of the working tube diameter,  $w_D$ , was found to be a maximum of  $\pm 1\%$ . The Reynolds number was calculated using Eq. (9) and its uncertainty was then evaluated

$$w_{Re} = \sqrt{\left(\frac{\partial Re}{\partial \dot{m}} \frac{\dot{m}}{Re} w_{\dot{m}}\right)^2 + \left(\frac{\partial Re}{\partial D} \frac{D}{Re} w_D\right)^2 + \left(\frac{\partial Re}{\partial \mu} \frac{\mu}{Re} w_{\mu}\right)^2} \quad \text{Eq. (12)}$$

where  $w_{Re}$  is the propagated uncertainty for the Reynolds number,  $w_{\dot{m}}$  is the uncertainty in mass flow rate and  $w_{\mu}$  is the uncertainty in fluid viscosity. The uncertainty in fluid viscosity was negligible as a standard book value was used at the working conditions. The uncertainty in mass flow rate,  $w_{\dot{m}}$ , was minimal at  $\pm 0.05\%$ . The total propagated uncertainty in Reynolds number was found to be a maximum of  $\pm 1\%$ . The friction factor for turbulent flow, Eq. (8), was used and the uncertainty was evaluated

$$w_f = \sqrt{\left(\frac{\partial f}{\partial \dot{m}} \frac{\dot{m}}{f} w_{\dot{m}}\right)^2 + \left(\frac{\partial f}{\partial Re} \frac{Re}{f} w_{Re}\right)^2 + \left(\frac{\partial f}{\partial D} \frac{D}{f} w_D\right)^2} \quad \text{Eq. (13)}$$

where  $w_f$  is the propagated uncertainty of the friction factor and was a maximum of  $\pm 0.27\%$ . The uncertainty in test section pressure drop was also estimated through a propagation of uncertainty approach. Tube diameter had a very strong influence on total pressure drop and was also the primary contributor to the total pressure drop uncertainty. Eq. (5) was used to evaluate pressure drop uncertainty

$$w_{\Delta P} = \sqrt{\left(\frac{\partial \Delta P}{\partial \dot{m}} \frac{\dot{m}}{\Delta P} w_{\dot{m}}\right)^2 + \left(\frac{\partial \Delta P}{\partial D} \frac{D}{\Delta P} w_D\right)^2 + \left(\frac{\partial \Delta P}{\partial f} \frac{f}{\Delta P} w_f\right)^2 + \left(\frac{\partial \Delta P}{\partial L} \frac{L}{\Delta P} w_L\right)^2 + \left(\frac{\partial \Delta P}{\partial \rho} \frac{\rho}{\Delta P} w_\rho\right)^2} \quad \text{Eq. (14)}$$

where  $w_{\Delta P}$  is the total propagated uncertainty of pressure drop measurements in the fully developed region of test and was a maximum of  $\pm 5\%$ .

## Chapter 4 - RESULTS AND DISCUSSION

### 4.1 Two-phase oil-water flows

#### 4.1.1 Experimental test matrix

After single-phase validation tests were completed, two-phase flow data were taken and analyzed. Tube size, material and fluid properties have been documented to have an effect on flow regime and pressure drop [20, 51]. The study investigated the effects of tube size and material on flow regime and pressure drop as shown in Table 4 and also the effects of oil viscosity, Table 5, on flow regime and pressure drop. The effects of tube diameter on flow regime and pressure drop were compared using a 2.1 mm and 3.7 mm borosilicate glass with Eötvös numbers of 0.2 and 0.6, respectively. The effect of tube materials were investigated using borosilicate glass, stainless steel, and Inconel. Two mineral oil, Parol 70 (P70) and Parol (100), of identical density and viscosity ratio close to two were investigated to understand the effects of oil viscosity on flow regime and pressure drop.

**Table 4 Fluid properties**

Properties	Water	Oil (Parol 70)	Oil (Parol 100)
Density at 24°C [kg/m <sup>3</sup> ]	$\rho_w = 997$	$\rho_o = 840$	$\rho_o = 847$
Viscosity at 23°C,40°C,40°C [mPa s]	$\mu_w = 1$	$\mu_o = 11.7$	$\mu_o = 20.8$
Oil-water interfacial tension [mN/m]	30-40		

**Table 5 Tube properties and Eötvös number**

Tube material	Tube ID (mm)	Eötvös	Oil velocity (m/s)	Water velocity (m/s)	Contact angle	Roughness (μm)
Borosilicate glass	2.1	0.2	0.85-6.82	0.21-6.77	18°	0.1
	3.7	0.6	0.28-3.32	0.07-4.99		
Stainless Steel	3.7	0.6	0.28-2.80	0.07-4.20	50°	5
Inconel	4	0.7	0.21-2.89	0.06-3.86	50°	3

### 4.1.2 Flow regime definitions

Determination of flow regimes were done by analyzing oil-water flow visualization videos captured at 1500–2000 fps and played back at 20 fps. Flow descriptions used in this study followed similar criteria found in the literature [6, 20, 32]. Various flow patterns were observed and were all categorized under four main flow types: stratified, annular, intermittent, and dispersed. Stratified flow is characterized by a single interface between two fluids flowing parallel to one another. Annular flow is characterized by circumferential interface between two fluids consisting of a continuous core phase and low pressure drop. Intermittent flow is characterized by one fluid flowing in discontinuous and sporadic segments within a continuous fluid. Dispersed flow is characterized by a scattered and dispersed fluid flowing within a continuous fluid. Each flow regime type displayed numerous configurations under different flow conditions, prompting additional flow descriptions. The additional flow descriptions were determined by each individual fluid behavior and were also based on sub descriptions found in the literature. In this study, flow regimes were categorized as follows:

Stratified flow,  $S$  (Figure 4): a two-layer flow with an interface between the two phases. The oil phase, in full contact with the tube wall, flows along the top and similarly the water phase flows along the bottom of the tube. Stratified flow displayed two different configurations: stratified-smooth ( $S_{smooth}$ ) with a smooth oil water interface and stratified-wavy ( $S_{wavy}$ ) with a wavy oil water interface. Stratified flow was the only flow regime to have oil in full contact with the top of the tube walls.

Annular flow,  $A$  (Figure 5): a separated flow consisting of the more viscous fluid (oil) flowing continuously in the core circumferentially contained by a film of the higher surface tension fluid (water) flowing in the annulus. Annular flow displayed four different configurations and are

described based on the oil core behavior: annular-stratified ( $A_{stratified}$ ), a small or large eccentric oil core with a thin upper water film; annular-wavy ( $A_{wavy}$ ), a wavy interface; annular churn ( $A_{churn}$ ), a highly sheared and wavy oil core with entrainment; annular-dispersed ( $A_{dispersed}$ ), water droplets dispersed and entrained in the oil core.

Intermittent flow,  $I$  (Figure 6): consists of periodic oil slugs and droplets flowing in a continuous water phase. Intermittent flow displayed four different configurations and are also categorized based on oil core behavior: intermittent-slug ( $I_{slug}$ ), short or long smooth oil capsules with smooth oil-water interface; intermittent-wavy ( $I_{wavy}$ ), sheared and wavy interface without any entrainment; intermittent-churn ( $I_{churn}$ ), sheared oil slugs with water in oil entrainment; intermittent dispersed ( $I_{dispersed}$ ) small oil droplets flowing in a continuous water phase.

Dispersed flow,  $D$  (Figure 7): consists of small dispersed oil droplets flowing through a continuous water phase. Dispersed flow displayed two different configurations: dispersed-churn ( $D_{churn}$ ), highly sheared oil slugs coupled with small oil droplets; dispersed-emulsion ( $D_{emulsion}$ ), fine oil droplets flowing in a continuous water phase or vice versa after phase change.

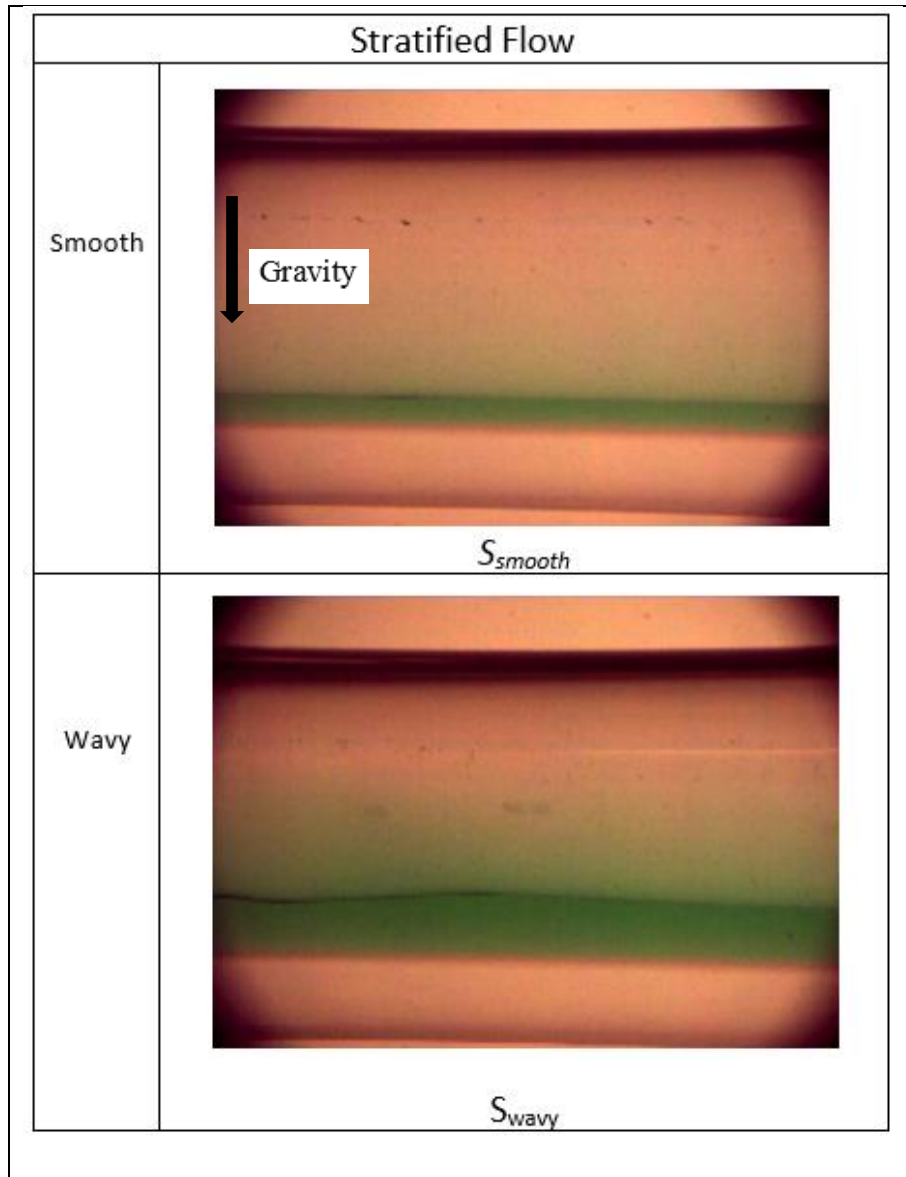


**Figure 4 Stratified flow regimes**

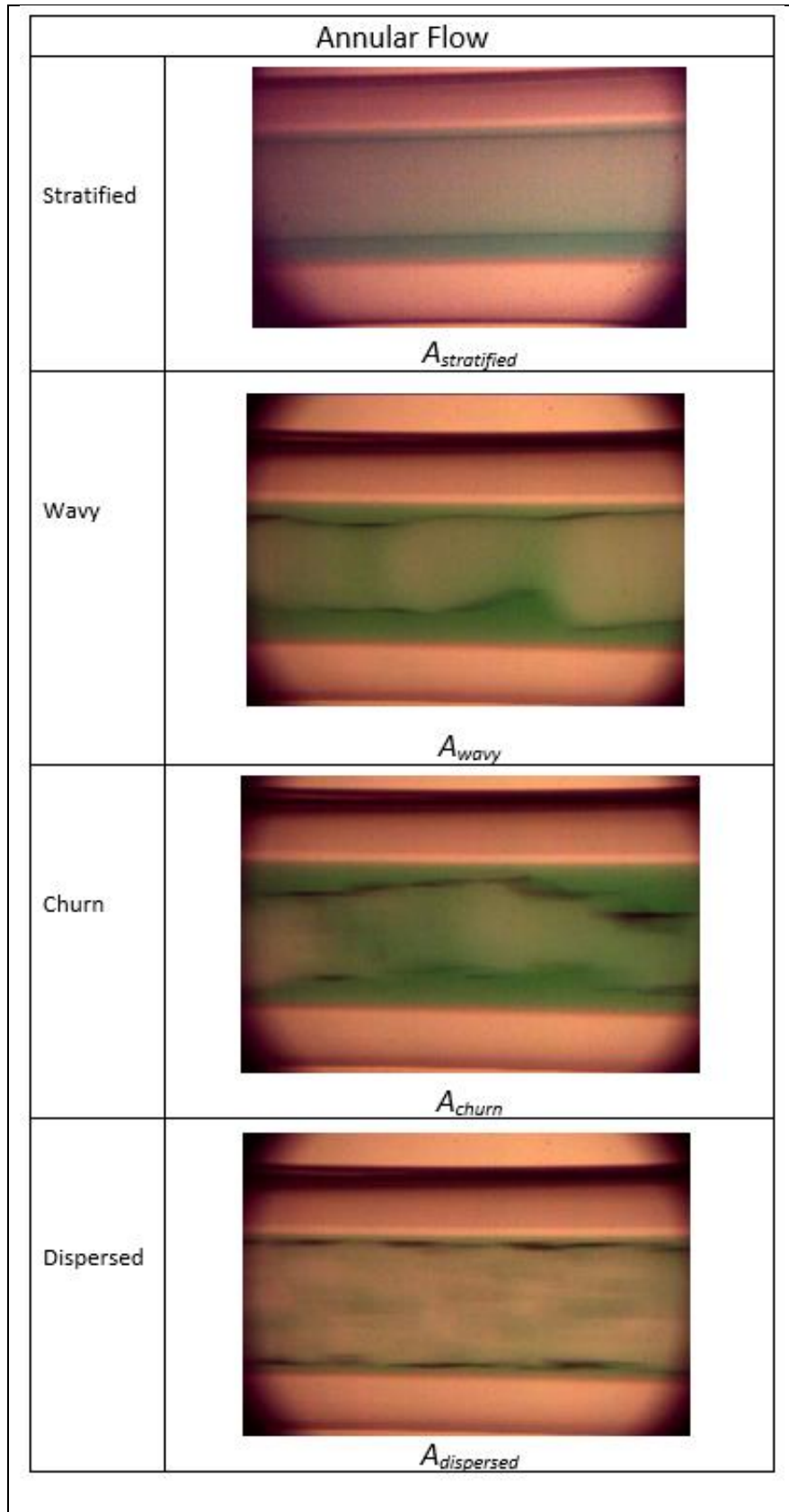
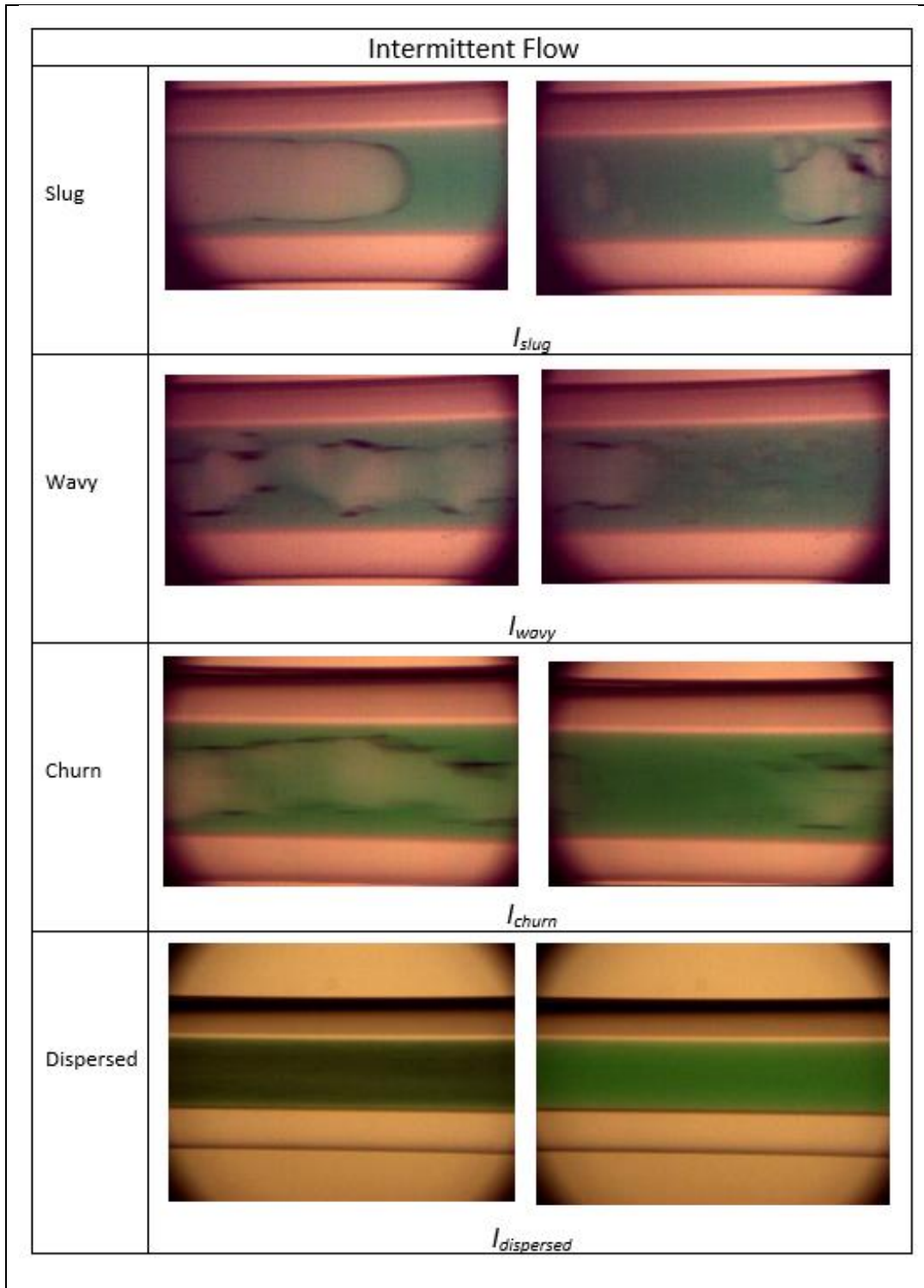
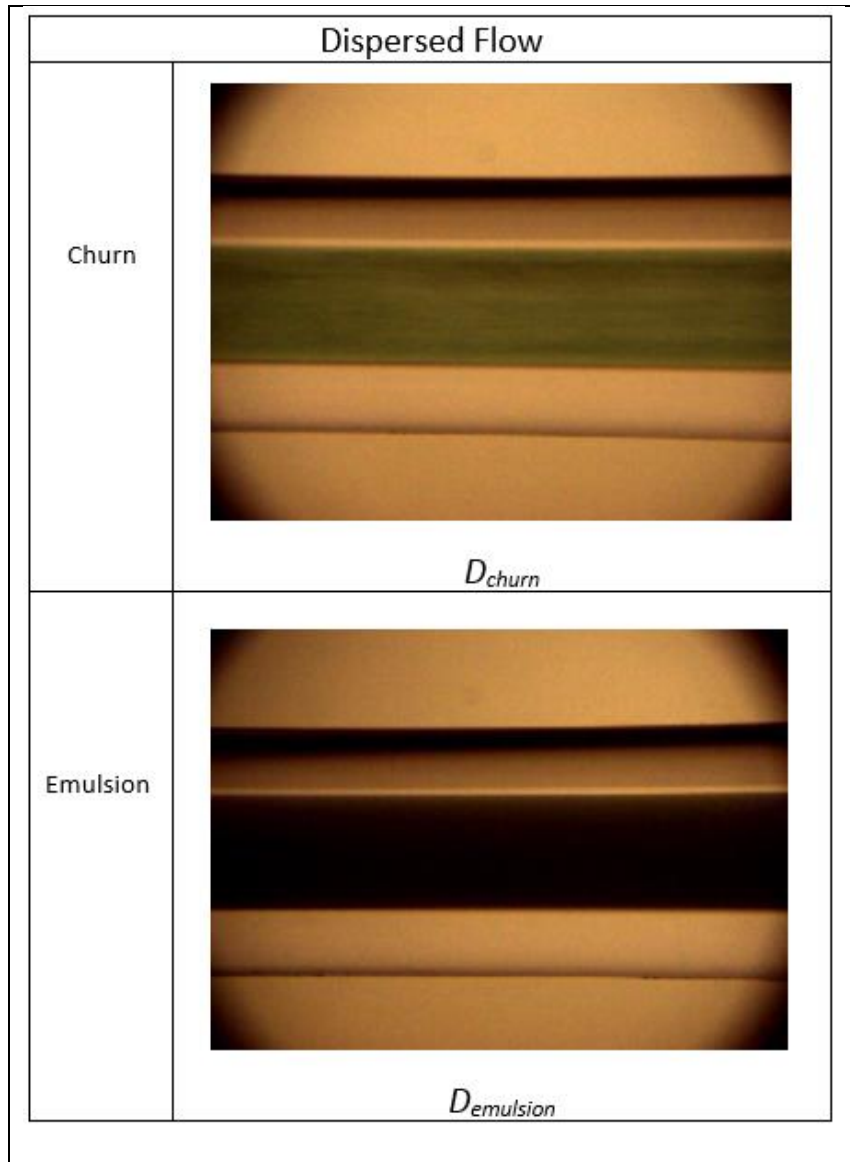


Figure 5 Annular flow regimes



**Figure 6 Intermittent flow regimes**



**Figure 7 Dispersed flow regimes**

### **4.1.3 Flow regime and pressure drop in 3.7-mm and 2.1-mm borosilicate glass**

#### **4.1.3.1 Effects of tube diameters**

The effects of tube diameter on flow regime and pressure drop was investigated. Two borosilicate glass tubes with inside diameters of 2.1-mm and 3.7-mm were explored and analyzed over a wide range of flow rates. Parol 70, the less viscous oil, was used for this comparison. Table 6 and Table 7 presents the tabulated data examined to generate the flow regime maps for each tube diameter along with the tabulated Reynolds and Capillary numbers. Using superficial oil and water velocities, Figure 8 and Figure 9 display the flow regime maps in the 2.1-mm and 3.7-mm tube respectively. The Eötvös number shown in table in Table 5 for each of the tubes were 0.2 and 0.6 respectively. In all of the flow data collected in this study, the oil phase was always in the laminar flow region,  $Re < 2300$ . The water phase however, transitioned to turbulent flow at higher flow velocities.

Pressures drop was a strong function of flow regime and was always higher in the smaller tube. The smaller and larger tube both displayed similar trends in flow regime transitions, however the decrease in tube diameter showed a significant effect on flow regime and pressure drop. Holistically, both tubes displayed the four dominant flow regimes. Starting with stratified flow at the lowest flow velocities, then annular flow as the superficial oil velocity increased or intermittent flow as the superficial water velocity increased, and finally, transition to dispersed flow occurred at the highest superficial oil and water velocities. Water flow remained in the laminar flow region for all cases of stratified flow and was in the turbulent region for all cases of dispersed flow recorded in the study. However, the water phase in annular and intermittent flows transitioned from laminar to turbulent and could be depicted by the transition from a smooth to wavy oil-water

interface. The differences in flow regime and pressure drop in the 2.1-mm and 3.7-mm tubes are as follows:

Stratified flow: The smaller, 2.1-mm, tube displayed a lower range of stratified flow compared to the larger, 3.7-mm, tube. The oil water interface during stratified flow was always smooth in the smaller tube. The stratified flow was only sustained at the lowest flow rates in the smaller tube and did not exist past superficial oil and water velocities of  $j_o=0.85$  m/s and  $j_w=0.36$  m/s respectively. The larger tube in comparison displayed different interfaces and sustained stratified flow for a wider range of flow rates than the smaller tube. In the larger tube, stratified flow existed at oil and water superficial velocities as high as of  $j_o=1.11$  m/s and  $j_w=0.37$  m/s respectively. Stratified flow is a gravity driven flow regime. Gravitational effects decrease as tube diameter decrease as shown by the Eötvös number. This explains the larger tube having a bigger range of stratified flow than the smaller tube.

Annular flow: The annular flow regime was different than stratified flow in both tubes. In the case of annular flow, the smaller tube displayed a slight wider range of annular flow compared to the larger tube. Both tubes were able to sustained the annular flow regime to about the same superficial oil and water velocities which were  $j_o=3.42$ m/s and  $j_w=1.68$  m/s respectively for the smaller tube and  $j_o=3.32$ m/s and  $j_w=1.68$  m/s respectively for the larger tube. The smaller tube displayed a larger range in annular flow because the onset of the annular flow regime took place at lower flow conditions than the larger tube. Annular flow appeared in the smaller tube at oil and water superficial velocities as low as  $j_o=0.85$  m/s and  $j_w=0.56$  m/s respectively, these flow conditions resulted in stratified flow in the larger tube. The lowest flow conditions resulting in annular flow in the larger tube were  $j_o=1.11$ m/s and  $j_w=0.47$  m/s. The oil-water interface in both tubes were fairly the same with the smaller tube having a couple more due to its wider range. The

onset of annular flow in the smaller tube showed a smooth interface and was stratified in nature while in most cases annular flow started with a wavy oil-water interface in the larger tube. As previously mentioned, the upper bound of annular flow was about the same for both tubes. They both displayed the annular-dispersed flow regime as flow conditions approached the upper bound.

Intermittent: Unlike annular flow, the upper bound for intermittent flow was a lot more different for both tubes. The smaller tube sustained intermittent flow at much higher water flow conditions i.e.  $j_w=7.63$  m/s and possibly beyond, Figure 8. While the collected data for the larger tube stops at water superficial velocity of  $j_w=2.59$  m/s the flow regime at this condition is intermittent-dispersed, showing the upper limit of intermittent flow in the larger tube. The intermittent flow regime oil-water interface, throughout the different stages of intermittent flow, was relatively similar for both tubes. The intermittent-slug flow manifested itself at lower flow conditions in both tubes and transitioned to churn and ultimately dispersed as water superficial velocity increased.

Dispersed: The dispersed flow regime occupied the highest flow velocities. The larger tube transitioned to disperse flow at lower flow conditions than the smaller tube. Dispersed flow initiated in the larger tube at superficial oil and water rates of  $j_o=2.22$  m/s and  $j_w=2.20$  m/s respectively, while the smaller tube displayed the onset of dispersed flow at superficial oil and water velocities of  $j_o=3.42$  m/s and  $j_w=3.39$  m/s respectively. The Capillary numbers for dispersed flow in the 2.1-mm tube ranged were  $0.8 < Ca < 1.25$  and  $1.15 < Ca < 2.30$  for the 3.7-mm tube. The Capillary numbers being above 1 indicate the dominant effects of viscous forces. The smaller tube was more influenced by surface tension forces compared to the larger tube. This could explain the larger tube transitioning at lower flow velocities.

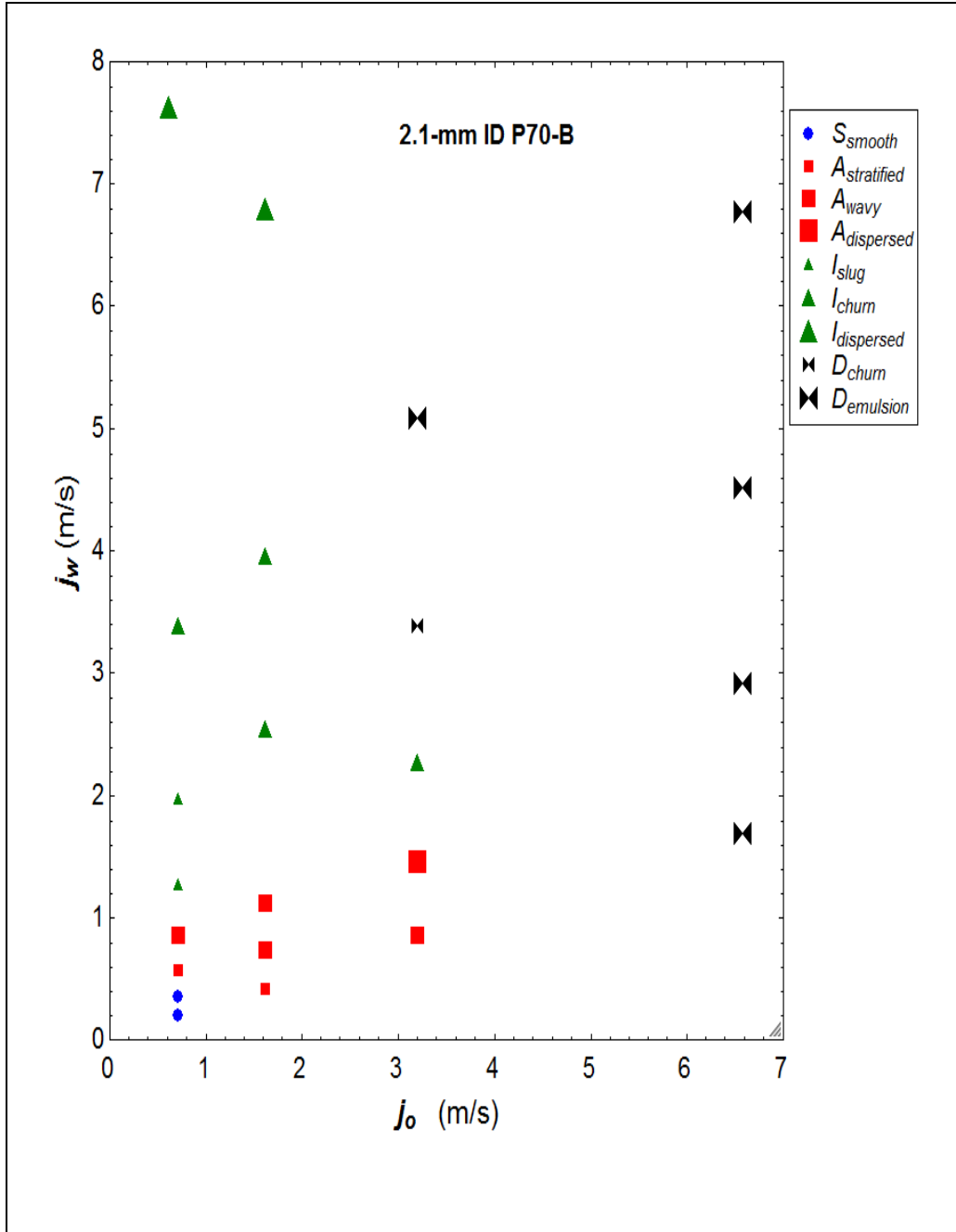


Figure 8 Flow regime map for the 2.1-mm borosilicate tube with Parol 70 oil



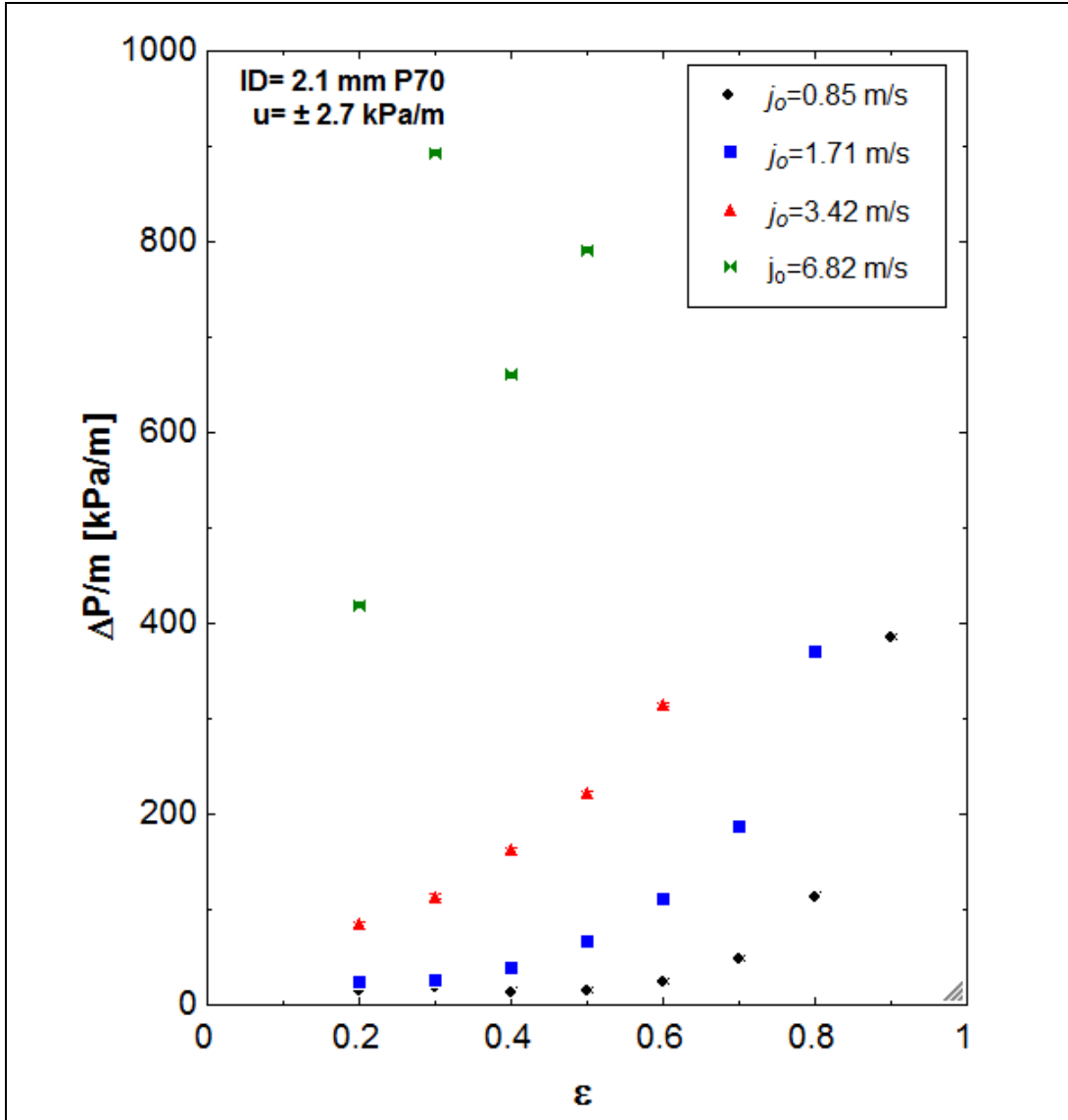


Figure 10 Pressure drops in 2.1-mm borosilicate glass tube with Parol 70 oil

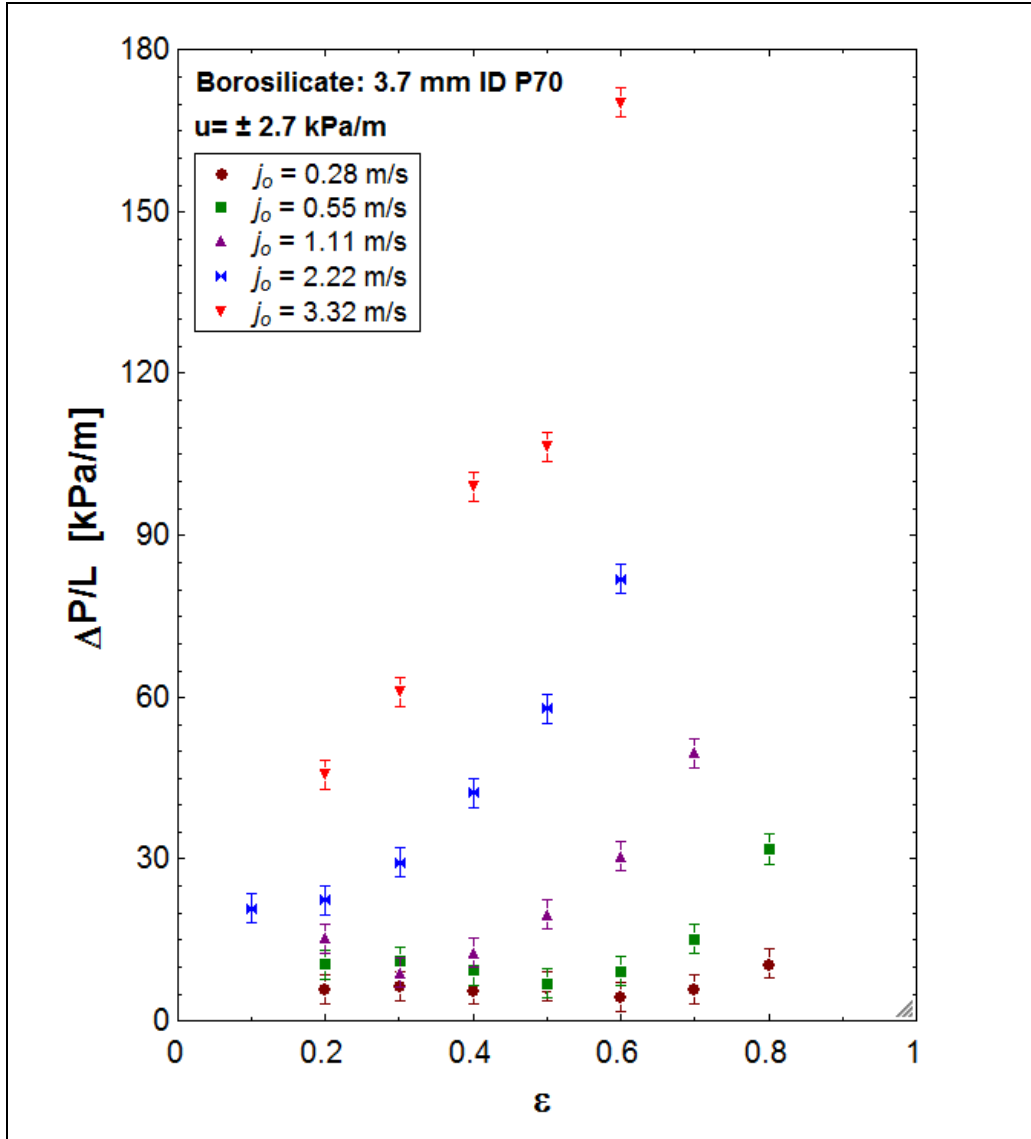


Figure 11 Pressure drops in the 3.7-mm borosilicate glass tube with Parol 70 oil

**Table 6 Flow regime map data for the 2.1-mm borosilicate glass tube with Parol 70**

2.1-mm ID P70						
Flow Regime	$j_o$ (m/s) [ $Re_o$ ]	$j_w$ (m/s) [ $Re_w$ ]	Ca	$\epsilon$	$\Delta P$ (kPa/m)	Flow Description
Stratified	0.85 [129]	0.21 [444]	0.28	0.2	17.3	smooth
		0.36 [763]	0.28	0.3	20.3	smooth
Annular	0.85 [129]	0.57 [1187]	0.28	0.4	15.6	stratified
		0.85 [1783]	0.29	0.5	15.8	wavy
	1.71 [259]	0.42 [881]	0.57	0.2	24.6	stratified
		0.73 [1534]	0.57	0.3	26.7	wavy
		1.12 [2354]	0.57	0.4	38.5	wavy
		1.68 [3531]	0.58	0.5	66.5	churn
	3.42 [518]	0.85 [1777]	1.13	0.2	84.4	wavy
		1.46 [3067]	1.13	0.3	113.7	dispersed
Intermittent	0.85 [129]	1.27 [2662]	0.29	0.6	25.3	slug
		1.97 [4134]	0.31	0.7	49.9	slug
		3.39 [7107]	0.35	0.8	115.1	churn
		7.63 [15993]	0.46	0.9	386.9	dispersed
	1.71 [259]	2.54 [5318]	0.59	0.6	111.2	churn
		3.96 [8294]	0.63	0.7	186.6	churn
		6.79 [14230]	0.70	0.8	370.7	dispersed
	3.42 [518]	2.27 [4758]	1.14	0.4	162.2	churn
Dispersed	3.42 [518]	3.39 [7114]	1.15	0.5	221.5	churn
		5.09 [10678]	1.19	0.6	314.8	emulsion
	6.82 [1033]	1.69 [3546]	2.25	0.2	418.9	emulsion
		2.91 [6106]	2.25	0.3	893.5	emulsion
		4.52 [9475]	2.27	0.4	660.3	emulsion
		6.77 [14185]	2.30	0.5	791	emulsion

**Table 7 Flow regime map data for the 3.7-mm borosilicate glass tube with Parol 70**

3.7-mm ID P70						
Flow Regime	$j_o$ (m/s) [Reo]	$j_w$ (m/s) [Rew]	Ca	$\epsilon$	$\Delta P$ (kPa/m)	Flow Description
Stratified	0.28 [74]	0.07 [255]	0.09	0.2	5.9	smooth
		0.12 [438]	0.10	0.3	6.5	smooth
		0.18 [672]	0.10	0.4	5.8	smooth
		0.28 [1022]	0.10	0.5	6.3	smooth
	0.55 [146]	0.14 [519]	0.19	0.2	10.4	smooth
		0.24 [871]	0.19	0.3	11	wavy
		0.37 [1370]	0.20	0.4	9.3	wavy
1.11 [295]	0.24 [897]	0.38	0.2	15.3	smooth	
Annular	1.11 [295]	0.47 [1750]	0.38	0.3	8.9	wavy
		0.74 [2726]	0.39	0.4	12.5	wavy
		1.11 [4092]	0.40	0.5	19.7	wavy
	2.22 [589]	0.28 [1034]	0.75	0.1	20.8	wavy
		0.56 [2051]	0.76	0.2	22.3	dispersed
		0.92 [3378]	0.77	0.3	29.3	dispersed
	3.32 [881]	0.83 [3065]	1.14	0.2	45.6	dispersed
Intermittent	0.28 [74]	0.42 [1542]	0.10	0.6	4.5	slug
		0.65 [2381]	0.11	0.7	5.9	slug
		1.11 [4093]	0.12	0.8	10.6	slug
	0.55 [146]	0.55 [2043]	0.20	0.5	6.9	slug
		0.83 [3066]	0.21	0.6	9.1	slug
		1.29 [4766]	0.22	0.7	15.1	slug
		2.22 [8170]	0.25	0.8	31.8	churn
	1.11 [295]	1.66 [6129]	0.42	0.6	30.4	churn
		2.59 [9535]	0.44	0.7	49.6	dispersed
	2.22 [589]	1.47 [5413]	0.78	0.4	42.3	churn
Dispersed	2.22 [589]	2.2 [8102]	0.80	0.5	57.9	churn
		3.32 [12239]	0.84	0.6	81.9	emulsion
	3.32 [881]	1.43 [5253]	1.15	0.3	60.9	churn
		2.22 [8176]	1.17	0.4	99	emulsion
		3.32 [12255]	1.21	0.5	106.4	emulsion
		4.99 [18400]	1.25	0.6	170.1	emulsion

#### 4.1.3.2 Effects of oil viscosity

The oils investigated in this study, Parol 70 (P70) and Parol 100 (P100), are mineral oils with a factor of two difference in viscosity with essentially the same fluid densities. Figure 12 shows a flow regime map comparing the two oil viscosities in the 2.1-mm and the 3.7-mm borosilicate glass tube. Overall flow regime trends were very much the same for both oils and the effects of fluid viscosity were not substantial, nonetheless fluid viscosity effects could be observed in flow regime transition boundaries and in the overall stability of flow regimes in both tubes diameter. In the 2.1-mm tube, Figure 13, at low superficial oil and water velocities both oils start out showing stratified flow before transitioning to annular flow as both superficial oil and water velocities are increased. The annular flow then transitions to intermittent flow at relatively low superficial oil and high water velocities for both P70 and P100. The flow then finally transitions to dispersed flow at relatively high oil and water superficial velocities. Stratified, annular, and intermittent flow patterns all had slightly larger ranges in P100 while dispersed flow dominated in P70. This is partially due to the less viscous fluid having the higher tendency to mix, thereby accelerating droplet formation and entrainment, promoting the transition to dispersed flow regime patterns. The trend is similar for the larger 3.7-mm tube, Figure 13, except at the lower flow velocities. At the lowest recorded flow velocities in the larger tube, the less viscous oil (P70), behaves like the smaller tube showing stratified flow; however, the more viscous oil (P100), starts out with intermittent flow before transitioning to stratified flow, this was the only occurrence showing intermittent, or any other flow regime, preceding stratified flow. Overall stratified flow displayed a wider range in P70 while the intermittent flow regime was dominant in P100, especially in the 3.7-mm tube. The ranges in annular and dispersed flow were about the same for both oils, with P70 showing a slightly larger range in its less stable annular flow regime ( $A_{churn}$ ,

*A*dispersed). Flow stability was based on fluid entrainment were flow without entrainment would be considered stable and vice versa. In general, P100 displayed higher flow regime stability, as discussed in the literature [6, 11, 12, 14, 18] . This is very apparent in the 2.1-mm tube, Figure 12, with the annular and dispersed flow regime at higher superficial oil and water flow velocities.

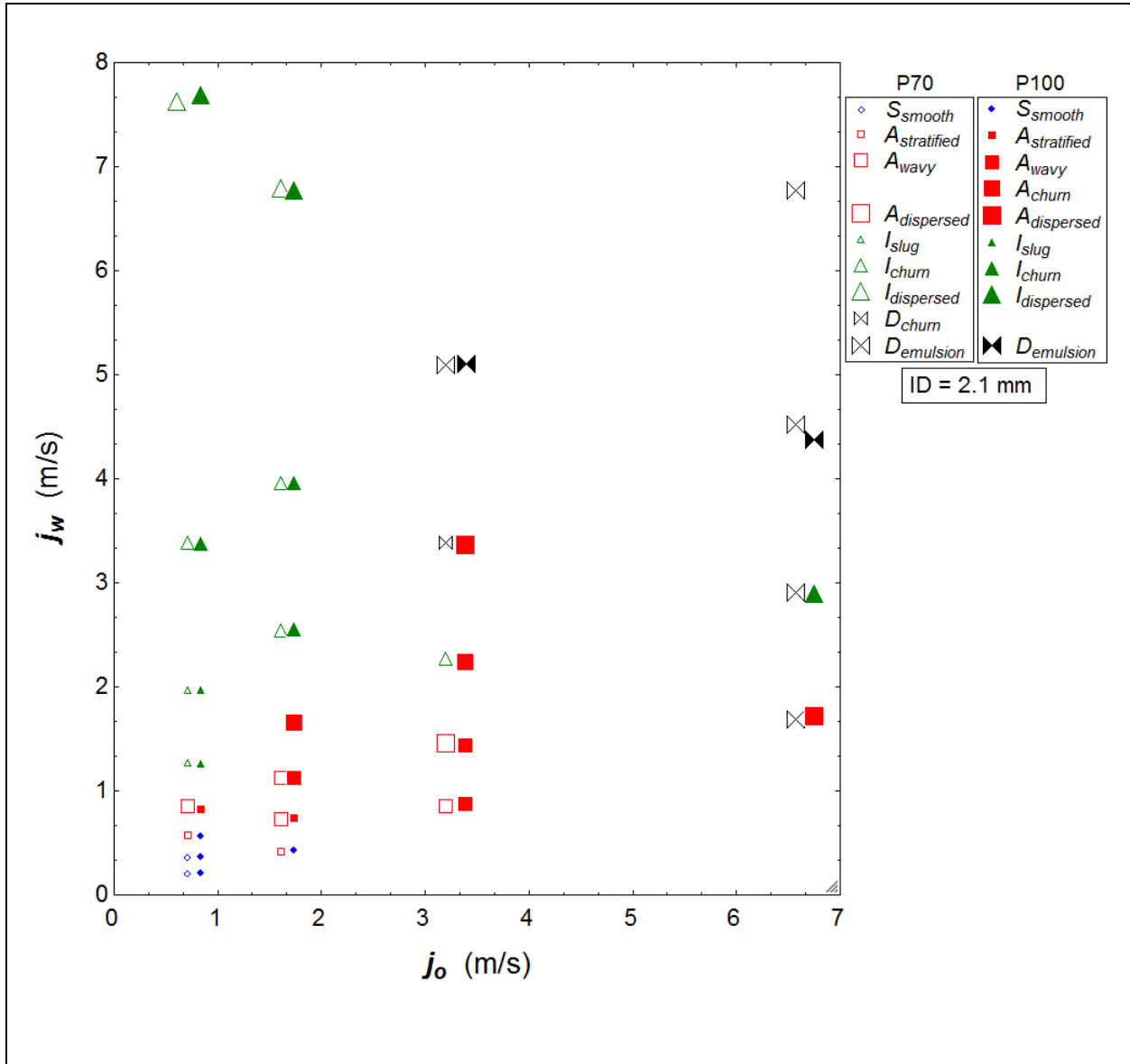


Figure 12 Flow regime map in the 2.1-mm borosilicate glass tube with Parol 70 and Parol 100 oil

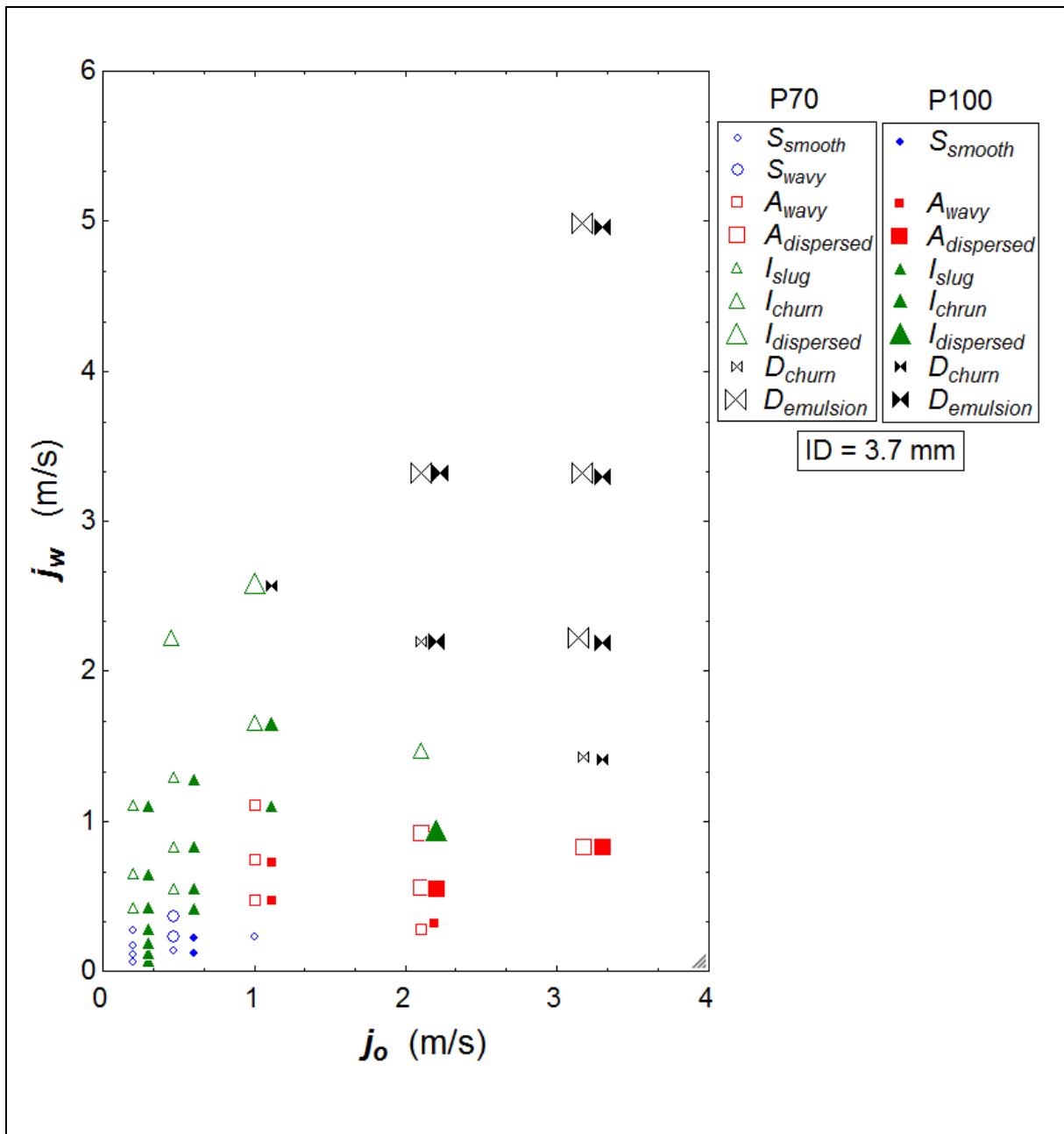


Figure 13 Flow regime maps in the 3.7-mm borosilicate glass tube with Parol 70 and Parol 100 oil

## 4.1.4 Flow regime and pressure drop in different tube materials

### 4.1.4.1 Comparison of flow in glass, stainless steel and Inconel tubes

The next step of the study was to examine different tube materials to see how they would compare to the borosilicate glass initially investigated. Two metal tubes, stainless steel and Inconel, were tested and compared to the borosilicate glass tube. Table 5 shows each of the tube dimensions and material properties along with their respective Eötvös numbers. The borosilicate glass and stainless steel tubes both had inside diameters measured at 3.7-mm while the Inconel had a slightly bigger tube diameter and was measured at 4-mm.

Flow regime maps for each of the tube materials were generated and are shown in Figure 14, Figure 15 and Figure 16. The four dominant flow regimes (i.e., stratified, annular, intermittent and dispersed flows) were present in all three tubes. Stratified flow existed at the lowest superficial oil and water velocities with  $S_{smooth}$  and  $S_{wavy}$  observed in all three tubes. The Inconel tube had the largest range of stratified flow which was anticipated noting that its Eötvös number was higher than the other tubes, Table 5. Intermittent flow populated the low oil and high water superficial velocity range and seemed to level off at water superficial velocities of about  $j_w = 3$  m/s for all three tubes. The annular flow regime range was fairly consistent throughout all three tube materials. The range in annular flow ranked lowest in the glass tube, followed by the stainless steel and then the Inconel with the highest range. Dispersed flow occurred at high superficial oil and water velocities and were consistent in all three tubes.

Flow transitions occurred at different flow conditions in each of the tubes. Starting with stratified flow, as superficial water velocity increased, flow regime transitioned to intermittent flow in the borosilicate glass and stainless steel. Stratified flow did not transition to intermittent flow in the Inconel tube. The Inconel tube transitioned from stratified directly to annular flow as

superficial water velocity increased. All three tubes displayed transition to annular flow as superficial oil velocity increased. Annular flow transitioned to intermittent at lower superficial water velocities. The upper bound in the annular flow regime was almost linear in nature with a positive slope for the stainless steel and Inconel tubes. The borosilicate glass however was also linear in nature but opposite, having a negative slope on the upper bound in annular flow. The annular flow regime did not sustain high superficial water velocities. At higher flow conditions, annular flow transitioned to dispersed flow. The transition to dispersed flow occurred at high oil velocity and relatively low superficial water velocity for the borosilicate glass while stainless steel and Inconel sustained slightly higher water flow rates. The stainless steel tube held the annular flow regime at slightly higher superficial water velocity than the glass tube and the Inconel held the regime at even higher velocities than the stainless steel.

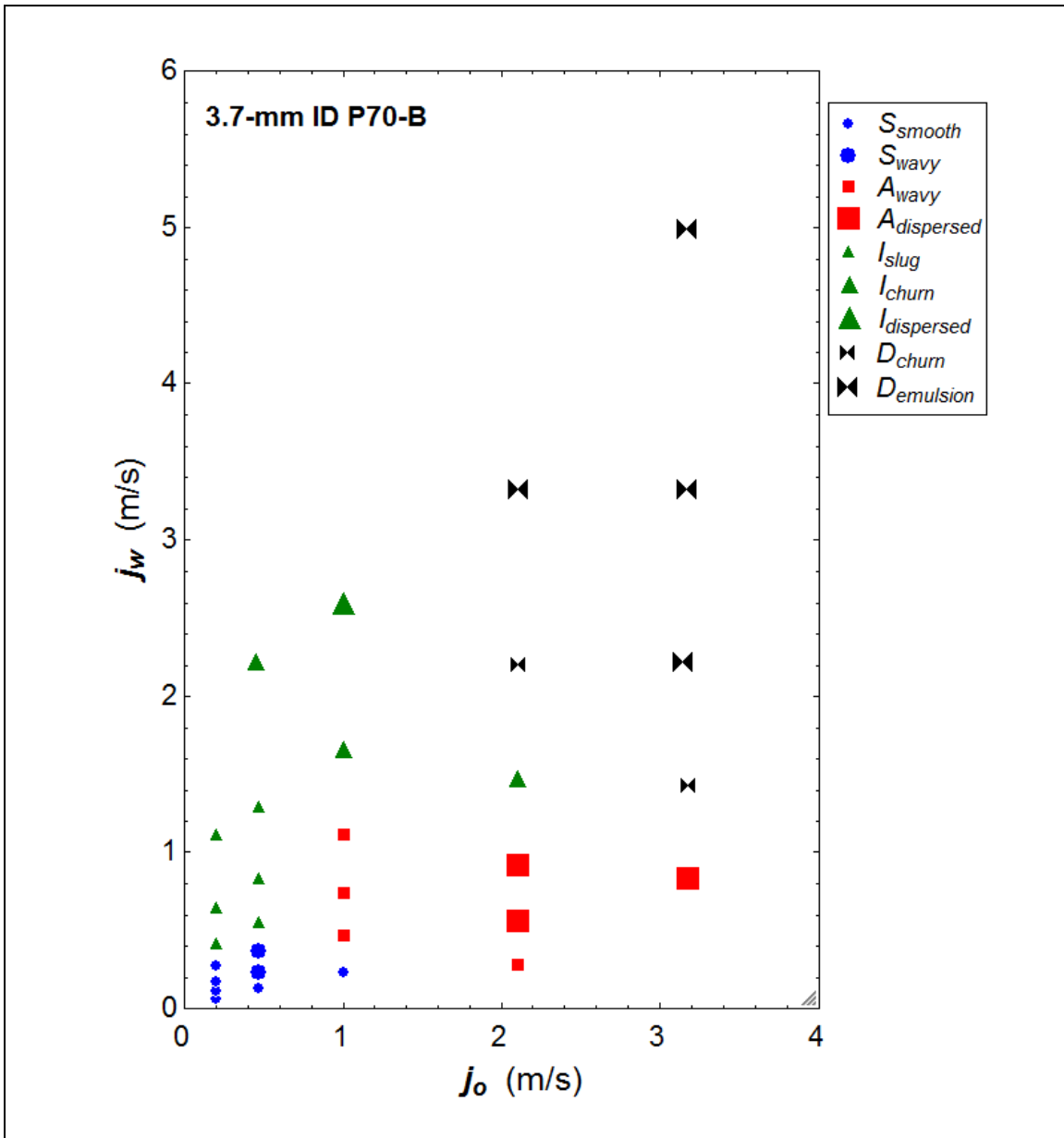


Figure 14 3.7-mm borosilicate glass tube flow regime map with Parol 70 oil

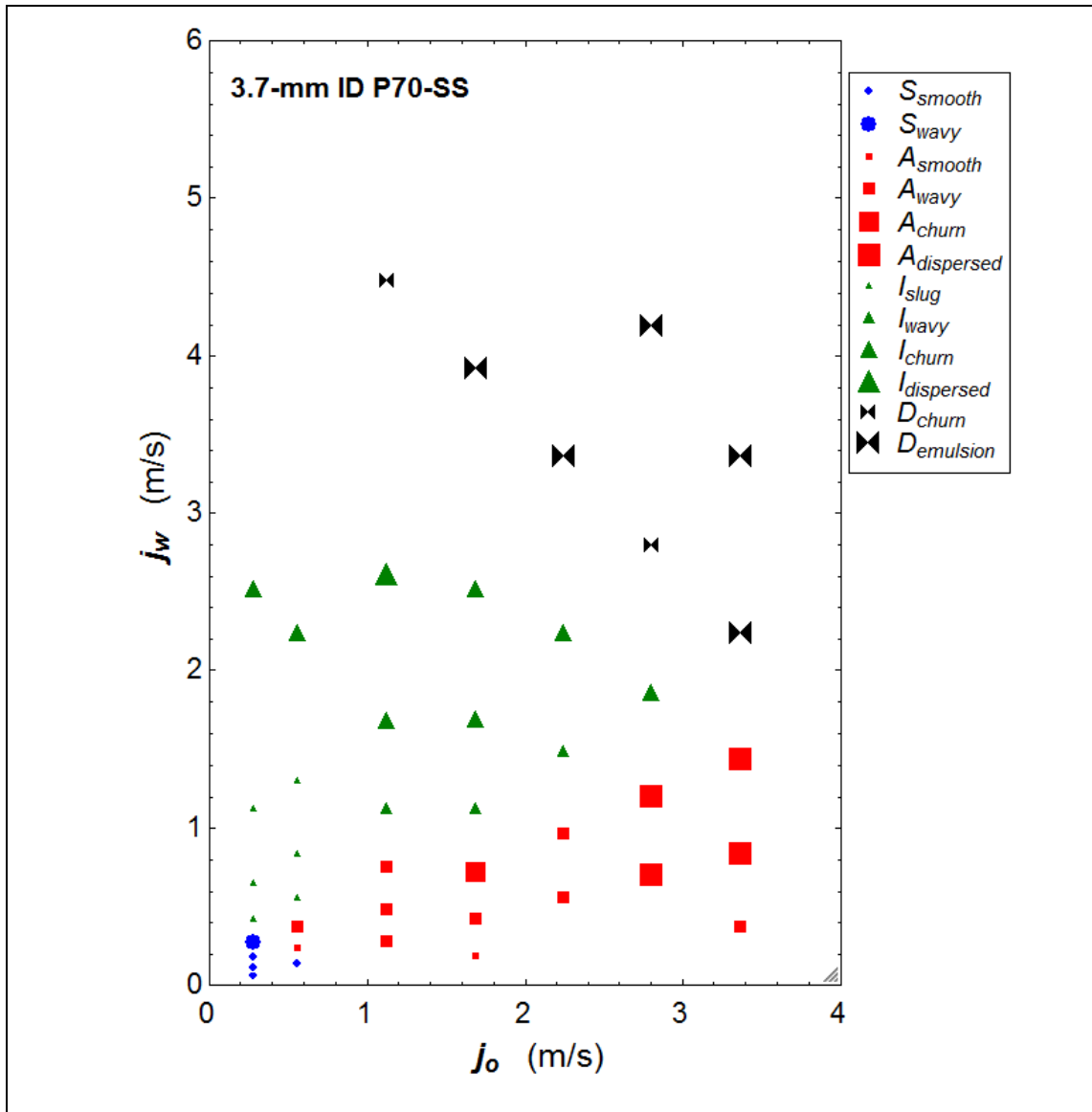


Figure 15 3.7-mm stainless steel tube flow regime map with Parol 70 oil

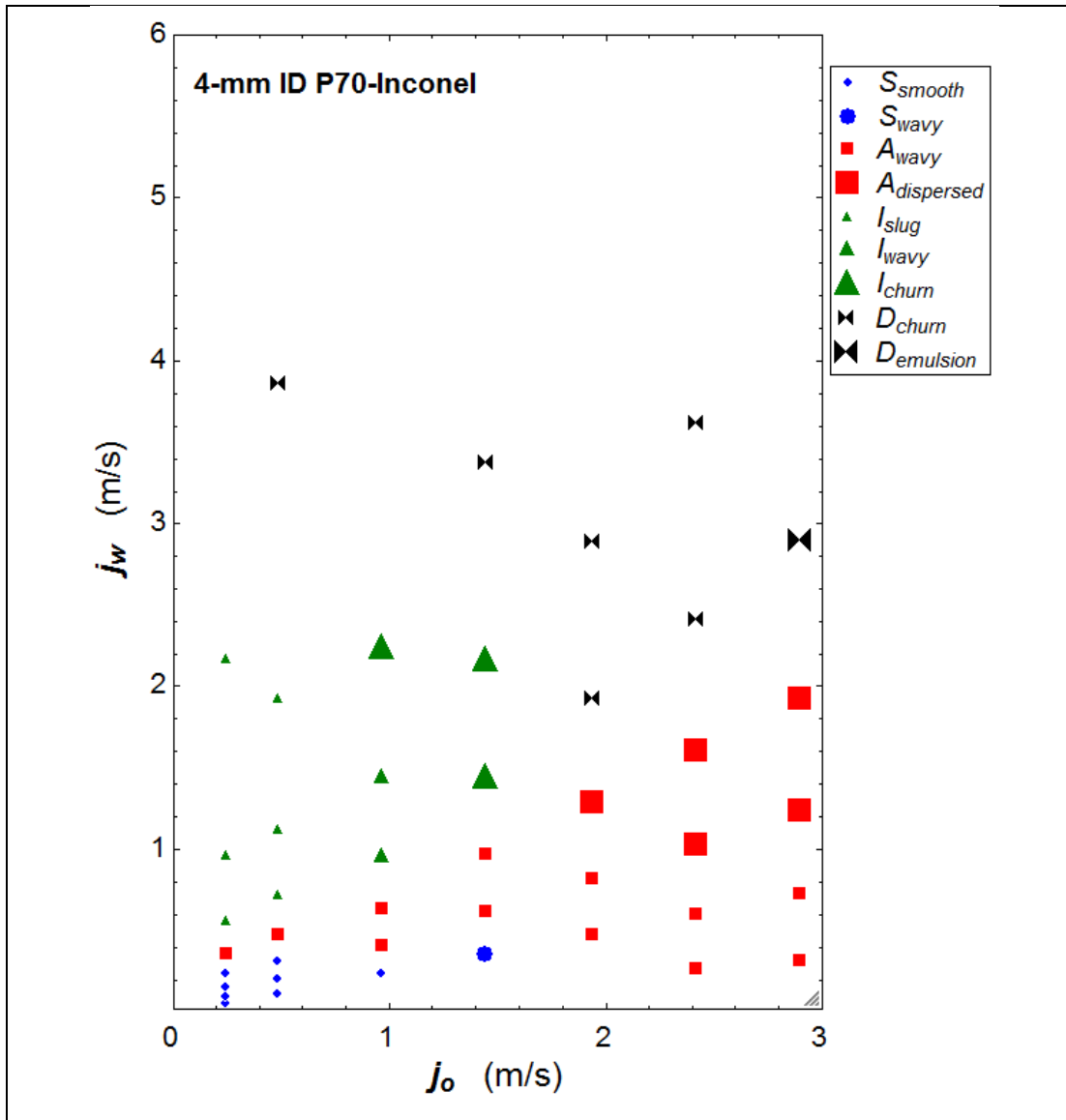


Figure 16 4.0 mm Inconel tube flow regime map with Parol 70 oil

#### 4.1.5 Pressure drop and flow observation regarding material differences

Flow regime in each tube material displayed different characteristics at similar flow conditions. Parol 70 is the oil used for all tube comparisons. Table 8 and Table 9 illustrates some of the flow configurations that occurred at the same oil and water superficial velocities in all three tubes. Figure 11, Figure 17 and Figure 18, show the pressure drop in the glass, stainless steel and Inconel tubes, respectively.

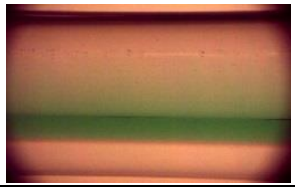
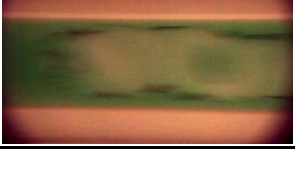
In Table 8, at an oil superficial velocity of  $j_o=0.3$  m/s and superficial water velocity of  $j_w=0.3$  m/s all three tubes display a stratified-smooth configuration and registered relatively similar pressure drops at 5.9, 6.8, and 7.3 kP/m for glass, stainless steel, and Inconel. With an increase in superficial water velocity of  $j_w=0.4$  m/s, the stratified oil phase is broken up, forming a stratified intermittent-slug flow ( $I_{slug}$ ) in the glass and stainless steel tube. The Inconel tube did not transition to intermittent flow. Flow in the Inconel alternated between stratified flow and a stratified-annular flow with a really thin water annulus at the top of the tube. The pressure drop recorded were 4.5, 7.1, 9.1 kP/m for the glass, stainless, steel and Inconel, respectively. At the same oil superficial velocity of  $j_o=0.3$  m/s, at  $j_w=0.7$  m/s, all three tubes displayed an intermittent-slug flow. Slug flow in stainless steel and Inconel is accompanied by smaller oil droplets. The pressure drops reflected the flow regime and were nearly identical at 10.6, 11.4, 10.1 kPa/m. At  $j_o=0.6$  m/s and  $j_w=0.2$  m/s, the glass and Inconel tube both display  $S_{smooth}$  flow while stainless steel displayed  $A_{stratified}$  flow. The pressure drops were 11.0, 9.7, 11.3 kPa/m for glass, stainless steel and Inconel, respectively. This observation, of annular yielding a lower pressure drop than stratified flow validated, validates the literature. Increasing the superficial water velocity to  $j_w=0.6$  m/s, the glass tube transitions to an intermittent flow highly resembling annular flow. The oil core would sustain for long periods of times and eventually breaking off, creating long slugs with a small gap in between slugs. This

*I<sub>slug</sub>* flow generated a pressure drop of 6.9 kPa/m which is 4.1 kPa/m lower than the previous flow condition at  $j_w=0.2$  m/s. Stainless steel stayed in the annular regime but transitioned to a wavy, *A<sub>wavy</sub>*, interface surrounded by small oil droplets and generated a pressure drop of 9.1 kPa/m. The Inconel tube transitioned to *A<sub>stratified</sub>* flow which decreased its pressure drop to 10.1 kPa/m. Increasing the water superficial velocity even higher to  $j_w=0.6$  m/s, flow in the glass and stainless tubes transitioned to *I<sub>churn</sub>* flow yield identical pressure drops at 31.8 and 32.1 m/s, respectively. Flow in the Inconel tube transitions to an *I<sub>wavy</sub>* flow regime and produces a pressure drop of 27.8 kPa/m. Increasing the oil superficial velocity to  $j_o=1.1$  m/s, at  $j_w=0.2$  m/s, all three tubes displayed annular flow. The glass tube shows a fairly concentric *A<sub>smooth</sub>* flow and has a pressure drop 8.9 kPa/m. Stainless steel displays a wavy interface surrounded by small oil droplets generating a pressure drop of 11.1  $\Delta$ Pa/m. Inconel displays a *A<sub>stratified</sub>* flow with a smooth interface and thin water annulus at the top of the tube. The *A<sub>stratified</sub>* flow in the Inconel tube generated pressure drop of 14.4  $\Delta$ Pa/m which was higher than the *A<sub>smooth</sub>* flow in the glass and the *A<sub>wavy</sub>* in the stainless steel. All three tubes maintained the annular flow regime when superficial water velocity increased to  $j_w=0.8$  m/s. The increase water superficial velocity induced flow transition in the glass from *A<sub>smooth</sub>* to *A<sub>wavy</sub>* which increased the pressure drop to 12.5  $\Delta$ Pa/m. Stainless steel remained at *A<sub>wavy</sub>* flow. The increase in velocity amplified the waves and generated more oil droplets which increased the pressure drop to 13.6  $\Delta$ Pa/m. The Inconel tube transitioned to a more concentric annular flow with a slightly wavy interface. The pressure drop decreased to 12.3 kPa/m in the Inconel.

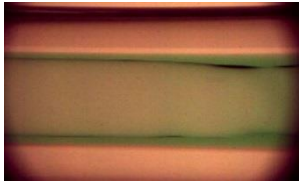
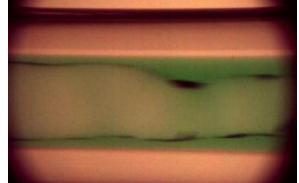
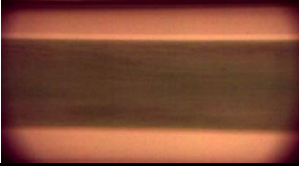
At a much more elevated oil superficial velocity of  $j_o=2.2$  m/s, looking at  $j_w=1.0$  m/s, similar to the previous flow conditions, all three tubes showed a form annular flow but this time they're all concentric in nature. The glass and the stainless steel tube displayed an *A<sub>churn</sub>* flow, where the concentric core is sheared causing small waves in the oil-water interface. The pressure drop for

both glass and stainless were identical at 29.3 and 29.8 kPa/m, respectively. The Inconel however, displayed a perfectly concentric annular flow with fairly smooth interface and generated a pressure drop of 25.8 kPa/m. At water superficial velocity of  $j_w=1.0$  m/s the glass and stainless steel tube continued to behave similarly as they both transition to  $I_{churn}$  flow. The glass generated a pressure drop of 57.9 kPa/m which was lower than the stainless steel at 63.7 kPa/m. The Inconel transitioned to  $A_{churn}$  flow and yielded a pressure drop of 52.1 kPa/m. At the highest oil superficial velocity recorded of  $j_o=3.4$  m/s, the three tubes displayed  $A_{dispersed}$  flow with concentric core and thin water annulus at a superficial water velocity of  $j_w=1.0$  m/s. The pressure drops generated were 45.6, 42.4, and 35.4 kPa/m where the Inconel had the lowest pressure drop, followed by the stainless steel and glass with the lowest pressure drop. As superficial water velocity increased to  $j_w=2.2$  m/s, the glass and stainless steel tube displayed an emulsion flow,  $D_{emulsion}$ , while the Inconel still showed a distinct water annulus flowing around a dispersed concentric oil core. The Inconel generated a 71.2 kPa/m pressure drop, which was again lower than the glass and stainless steel. However, at this flow condition, the glass generated pressure drop of 99.0 kPa/m which was higher than the stainless steel at 85.6 kPa/m

**Table 8 Flows regime in glass, stainless steel and Inconel at similar oil superficial velocities ( $j_o = 0.3$  and  $0.6$  m/s) and same water input ratio**

$j_o$ (m/s)	$j_w$ (m/s)	Glass	Stainless Steel	Inconel
0.3	0.3			
	0.4			
	0.7			
0.6	0.2			
	0.6			
	2.2			

**Table 9 Flow regime in glass, stainless steel and Inconel at similar superficial oil velocities ( $j_o = 1.1, 2.2$  and  $3.4$  m/s) and same water input ratio**

$j_o$ (m/s)	$j_w$ (m/s)	Glass	Stainless Steel	Inconel
1.1	0.5			
	0.8			
2.2	1.0			
	2.2			
3.4	0.8			
	2.2			

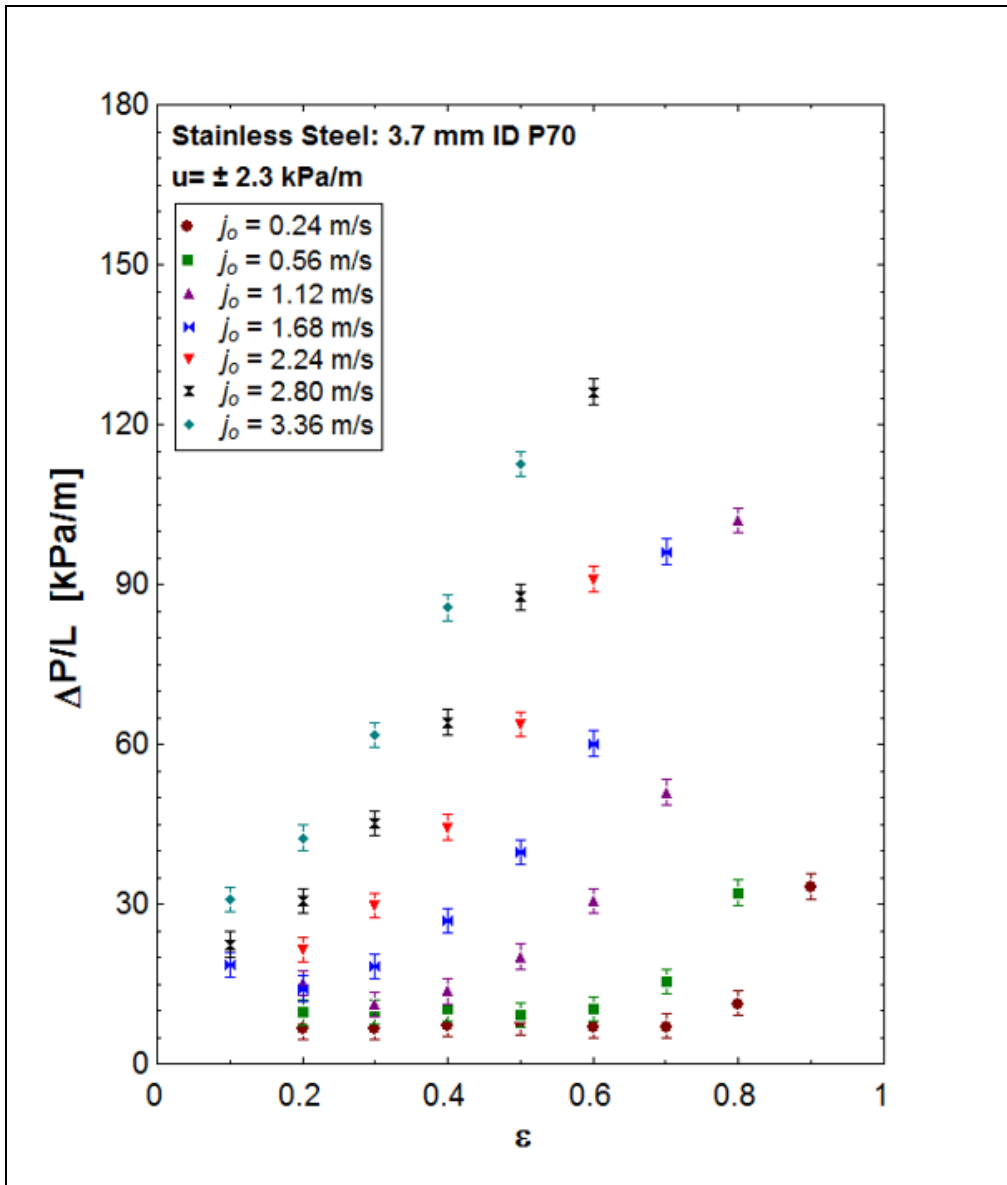


Figure 17 Pressure drops in the 3.7-mm stainless steel with Parol 70 oil

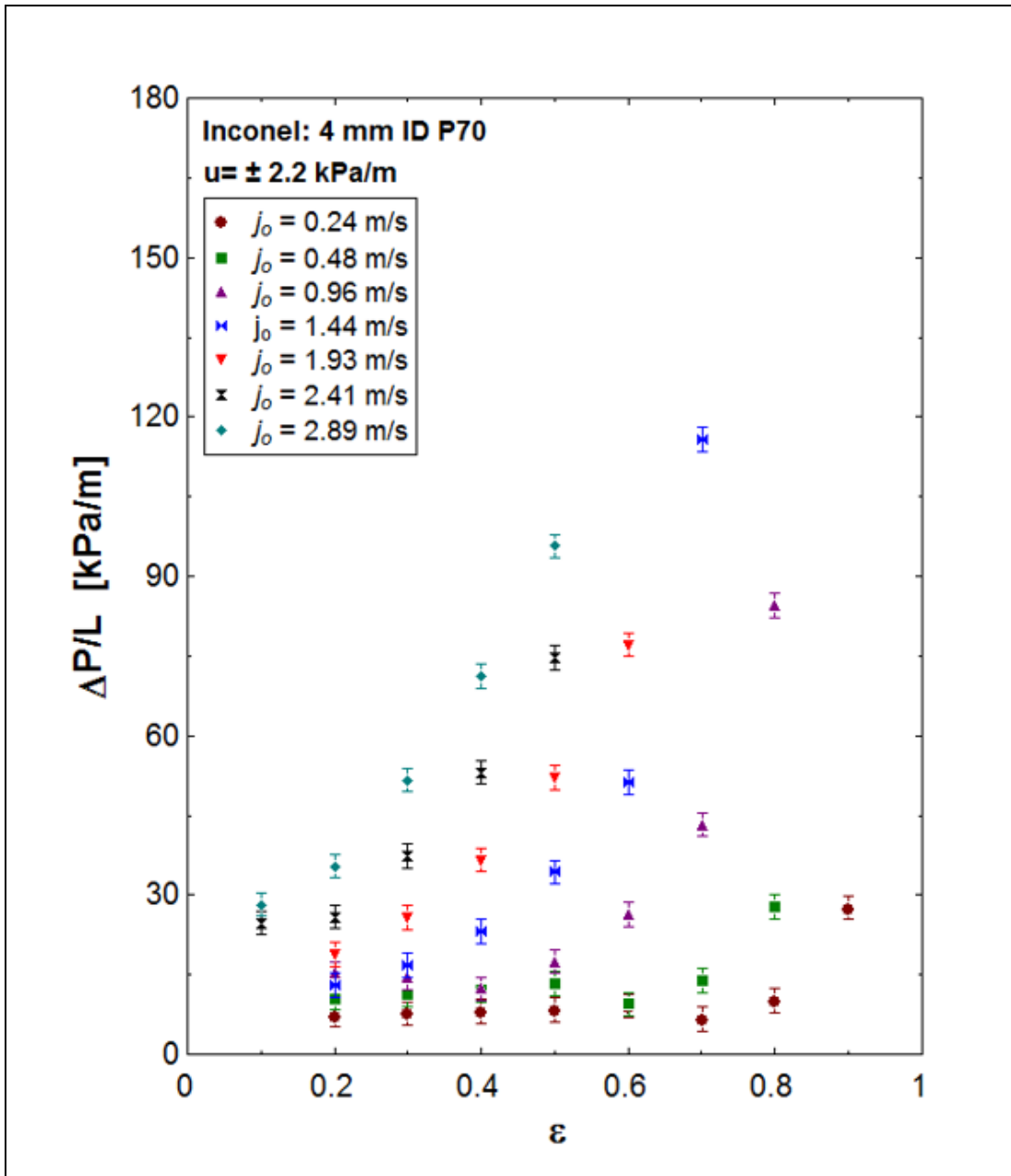


Figure 18 Pressure drops in the 4.0-mm Inconel tube with Parol 70 oil

## Chapter 5 - CONCLUSIONS AND FUTURE WORK

### 5.1 Conclusions

There is a need to improve current desalting techniques for deep sea drilling applications, as offshore drilling continues to expand due to technological advances in oil discovery at deeper regions in the ocean sea floor. Two-phase liquid-liquid flows have not received the same attention as gas-liquid flows over the years despite their importance in the petroleum and petrochemical industries. Gas-liquid systems have been extensively investigated and are well documented. However, models developed for gas-liquid systems are not readily interchangeable with liquid-liquid flows since oil-water flows typically have large viscosity differences and similar densities, whereas liquid-vapor flows often have large density differences and more comparable viscosities [17, 32].

The purpose of this research was to investigate the effects of tube diameter, oil viscosity, and tube material on flow regime and pressure drop in mini-channel oil-water flows. A horizontal, closed loop experimental apparatus was constructed and adiabatic oil-water flows were studied and visualized. The experimental apparatus was validated through single-phase water tests using 2.1-mm and 3.7-mm borosilicate glass tubes. The analytical pressure drop model showed excellent agreement with the experimental results with a mean percent error of under 5% for both diameter tubes. Upon single-phase validation, two-phase oil-water flows were then investigated. Borosilicate glass tubes of 2.1-mm and 3.7-mm were used to investigate the effects of tube diameter. To investigate the effects of oil viscosity, the oil used in this research were mineral oil Parol 70 (P70) and Parol 100 (P100) with viscosities of 11.7 and 20.8 mPa-s respectively. Lastly, borosilicate glass and stainless steel, both having a tube diameter of 3.7-mm, and Inconel with a

tube diameter of 4-mm were used to investigate the effects of tube material on flow regime and pressure drop.

The main conclusions of this study are as follows:

- The flow regimes visualized in the study were analogous to what was found in the literature and were categorized under four main flow types: stratified, annular, intermittent and dispersed. Each flow regime type displayed numerous configurations under different flow conditions. A list of flow regime definition along with additional flow descriptions was provided.
- The effects of tube diameters were investigated using mineral oil P70. Flow regime maps were created and pressure drops were graphed. The calculated Eötvös numbers were 0.2 and 0.6 for the 2.1-mm and 3.7-mm tube, respectively. The pressure drop was a strong function of flow regime and was always higher in the smaller tube. Both tubes displayed the four dominant flow regimes and had similar transition points, although the 2.1-mm displayed a lower stratified flow range compared to the 3.7-mm tube. This trend agreed with the literature as researchers have found that stratified flow, a gravity driven flow, is not attainable in micro-channels flows and only span a small range in mini-channels [6, 10, 11, 14, 32, 38, 39].
- Annular flow was similar for both tubes. The 2.1-mm tube displayed a slightly wider range of annular flow compared to the 3.7-mm tube. A significant change in pressure drop was always observed as flow would transition to annular flow. This is commensurate with previous work; Brauner et al. [6] developed a classification of liquid-liquid flow patterns in horizontal tubes according to the dimensionless Eötvös number and found that at small

tube diameters (e.g.,  $E_{OD} < 1$ ) interfacial tension effects are dominant and annular flows occur for a wider range of flow conditions.

- The smaller tube also sustained intermittent flow at much higher water flow conditions than the larger tube. Dispersed flow occupied the highest flow velocities on both tubes. The onset of dispersion occurred a lower flow conditions in the larger tube.
- The effects of oil viscosity were investigated in both 2.1-mm and 3.7-mm tube using P70 and P100. Overall flow regime trends were similar for both oils and the effects of fluid viscosity were not substantial; nonetheless, fluid viscosity effects could be observed in flow regime transition boundaries and in the overall stability of flow regimes in both tubes diameter. In general, P100 displayed higher flow regime stability following what is found in the literature [6, 11, 12, 14, 18]. Oil viscosity comparison graphs were provided. Overall oil-water flows in all three tube material behaved very similarly, however, distinct differences were observed in flow regime range across the tube. The Inconel tube had the largest range of stratified flow which was anticipated noting that its Eötvös number was higher than the other tubes. The annular flow regime range ranked lowest in the glass tube, followed by the stainless steel and then the Inconel with the highest range. The transition to dispersed flow occurred at high oil velocity and relatively low superficial water velocity for the borosilicate glass while stainless steel and Inconel sustained slightly higher water flow rates. At same oil and water superficial velocities and relatively the same flow regime, stainless steel and Inconel always displayed higher pressure drop than the glass tube. However, pressure drop was a strong function of flow regime and each flow regime dictated the range of pressure drop the flow generated.

## 5.2 Future work

There are several opportunities for future research. Manufacturing and implementing surface tension driven annular flow oil-water separation devices is still in the early research stages. This research provided the first steps which was to have a general understanding of oil-water flow regimes and pressure drop in mini-channel and possible conditions are suitable to sustain annular flow in small channels.

Future work using current data may include:

- Thorough analysis on effects of viscous, inertial, capillary and surface tension forces using dimensionless parameters.
- Developing models to best capture flow regime transitions and pressure drop
- Investigating the onset of interface entrainment focusing on Kelvin-Helmholtz and Rayleigh-Taylor instabilities.

Future work for the entire project would focus specifically on annular flow regime:

- Investigating fouling in mini-channels and the effect of tube roughness and hydrophobicity on oil-water annular flow.
- Investigating effects of oil viscosity in medium to heavy crude oil API gravity 30 °API to °API 10

## References

- [1] EIA, U. S., 2016, "U.S. Energy Facts Explained. Consumption & Production."
- [2] EIA, U. S., 2016, "Offshore production nearly 30% of global crude oil output in 2015."
- [3] Chakhmakchev, A., and Rushworth, P., 2010, "Global overview of offshore oil & gas operations for 2005-2009," *Offshore*, 70(5), pp. 32-38.
- [4] Cameron, 2010, "Process Systems- NATCO Electro-Dynamic Desalter (EED)."
- [5] Hadžiabdić, M., and Oliemans, R., 2007, "Parametric study of a model for determining the liquid flow-rates from the pressure drop and water hold-up in oil–water flows," *International Journal of Multiphase Flow*, 33(12), pp. 1365-1394.
- [6] Brauner, N., and Maron, D. M., "Classification of Liquid-Liquid Two-Phase Flow Systems and The Prediction of Flow Pattern Maps," *Proc. 2nd International Symposium on Two-Phase Flow Modeling and Experimentation–ISTP*, pp. 747-754.
- [7] Lovick, J., 2004, "Horizontal, oil-water flows in the dual continuous flow regime," University of London.
- [8] Hall, A., and Hewitt, G., 1993, "Application of two-fluid analysis to laminar stratified oil-water flows," *International journal of multiphase flow*, 19(4), pp. 711-717.
- [9] Mandal, T., Chakrabarti, D., and Das, G., 2007, "Oil water flow through different diameter pipes: similarities and differences," *Chemical Engineering Research and Design*, 85(8), pp. 1123-1128.
- [10] Russell, T., and Charles, M., 1959, "The effect of the less viscous liquid in the laminar flow of two immiscible liquids," *The Canadian Journal of Chemical Engineering*, 37(1), pp. 18-24.
- [11] Charles, M. E., Govier, G. t., and Hodgson, G., 1961, "The horizontal pipeline flow of equal density oil-water mixtures," *the Canadian Journal of Chemical engineering*, 39(1), pp. 27-36.
- [12] Bannwart, A. C., Rodriguez, O. M., de Carvalho, C. H., Wang, I. S., and Vara, R. M., 2004, "Flow patterns in heavy crude oil-water flow," *Journal of energy resources technology*, 126(3), pp. 184-189.
- [13] Bannwart, A., Rodriguez, O., Trevisan, F., Vieira, F., and De Carvalho, C., 2009, "Experimental investigation on liquid–liquid–gas flow: flow patterns and pressure-gradient," *Journal of petroleum science and engineering*, 65(1), pp. 1-13.
- [14] Al-Wahaibi, T., and Angeli, P., 2007, "Transition between stratified and non-stratified horizontal oil–water flows. Part I: Stability analysis," *Chemical Engineering Science*, 62(11), pp. 2915-2928.
- [15] Al-Wahaibi, T., and Angeli, P., 2009, "Predictive model of the entrained fraction in horizontal oil–water flows," *Chemical Engineering Science*, 64(12), pp. 2817-2825.
- [16] Angeli, P., and Hewitt, G., 2000, "Flow structure in horizontal oil–water flow," *International journal of multiphase flow*, 26(7), pp. 1117-1140.
- [17] Atmaca, S., Sarica, C., Zhang, H.-Q., and Al-Sarkhi, A., "Characterization of oil water flows in inclined pipes," *Proc. SPE Annual Technical Conference and Exhibition, Society of Petroleum Engineers*.
- [18] Brauner, N., and Ullmann, A., 2002, "Modeling of phase inversion phenomenon in two-phase pipe flows," *International Journal of Multiphase Flow*, 28(7), pp. 1177-1204.
- [19] Cobos, S., Carvalho, M., and Alvarado, V., "Flow of Oil-Water Emulsion Through Constricted Capillary Tubes," *Proc. The XV international congress on rheology: The Society of Rheology 80th Annual Meeting, AIP Publishing*, pp. 997-999.

- [20] Coleman, J. W., and Garimella, S., 2003, "Two-phase flow regimes in round, square and rectangular tubes during condensation of refrigerant R134a," *International Journal of Refrigeration*, 26(1), pp. 117-128.
- [21] Das, G., Chakrabarti, D., and Ray, S., 2005, "Pressure drop in liquid-liquid two phase horizontal flow: experiment and prediction," *Chemical Engineering and Technology*, 28(9), pp. 1003-1009.
- [22] Edomwonyi-Otu, L. C., and Angeli, P., 2015, "Pressure drop and holdup predictions in horizontal oil–water flows for curved and wavy interfaces," *Chemical Engineering Research and Design*, 93, pp. 55-65.
- [23] Ismail, A. S. I., Ismail, I., Zoveidavianpoor, M., Mohsin, R., Piroozian, A., Misnan, M. S., and Sariman, M. Z., 2015, "Experimental investigation of oil–water two-phase flow in horizontal pipes: Pressure losses, liquid holdup and flow patterns," *Journal of Petroleum Science and Engineering*, 127, pp. 409-420.
- [24] Joseph, D. D., Bai, R., Chen, K., and Renardy, Y. Y., 1997, "Core-annular flows," *Annual Review of Fluid Mechanics*, 29(1), pp. 65-90.
- [25] Salim, A., Fourar, M., Pironon, J., and Sausse, J., 2008, "Oil–water two-phase flow in microchannels: Flow patterns and pressure drop measurements," *The Canadian Journal of Chemical Engineering*, 86(6), pp. 978-988.
- [26] McKibben, M. J., Gillies, R. G., and Shook, C. A., 2000, "A laboratory investigation of horizontal well heavy oil—water flows," *The Canadian Journal of Chemical Engineering*, 78(4), pp. 743-751.
- [27] Rodriguez, O., and Oliemans, R., 2006, "Experimental study on oil–water flow in horizontal and slightly inclined pipes," *International Journal of Multiphase Flow*, 32(3), pp. 323-343.
- [28] Taitel, Y., and Dukler, A., 1976, "A model for predicting flow regime transitions in horizontal and near horizontal gas-liquid flow," *AIChE Journal*, 22(1), pp. 47-55.
- [29] Tsaoulidis, D., and Angeli, P., 2016, "Effect of channel size on liquid-liquid plug flow in small channels," *AIChE Journal*, 62(1), pp. 315-324.
- [30] Tsaoulidis, D., Dore, V., Angeli, P., Plechkova, N. V., and Seddon, K. R., 2013, "Flow patterns and pressure drop of ionic liquid–water two-phase flows in microchannels," *International Journal of Multiphase Flow*, 54, pp. 1-10.
- [31] Zhao, Y., Chen, G., and Yuan, Q., 2006, "Liquid-liquid two-phase flow patterns in a rectangular microchannel," *AIChE journal*, 52(12), pp. 4052-4060.
- [32] Brauner, N., 2003, "Liquid-liquid two-phase flow systems," *Modelling and Experimentation in Two-Phase Flow*, Springer, pp. 221-279.
- [33] Kashid, M., Renken, A., and Kiwi-Minsker, L., 2011, "Influence of flow regime on mass transfer in different types of microchannels," *Industrial & Engineering Chemistry Research*, 50(11), pp. 6906-6914.
- [34] Jovanović, J., Zhou, W., Rebrov, E. V., Nijhuis, T., Hessel, V., and Schouten, J. C., 2011, "Liquid–liquid slug flow: hydrodynamics and pressure drop," *Chemical Engineering Science*, 66(1), pp. 42-54.
- [35] Kashid, M., Harshe, Y., and Agar, D. W., 2007, "Liquid– liquid slug flow in a capillary: an alternative to suspended drop or film contactors," *Industrial & Engineering Chemistry Research*, 46(25), pp. 8420-8430.
- [36] Gupta, R., Leung, S. S., Manica, R., Fletcher, D. F., and Haynes, B. S., 2013, "Hydrodynamics of liquid–liquid Taylor flow in microchannels," *Chemical Engineering Science*, 92, pp. 180-189.

- [37] Das, G., Kannan, A., and Ray, S., 2016, "Liquid-liquid flow patterns in reduced dimension based on energy minimization approach," *AIChE Journal*, 62(1), pp. 287-294.
- [38] Balakhrisna, T., Ghosh, S., Das, G., and Das, P., 2010, "Oil–water flows through sudden contraction and expansion in a horizontal pipe–Phase distribution and pressure drop," *International Journal of Multiphase Flow*, 36(1), pp. 13-24.
- [39] Hasson, D., Mann, V., and Nir, A., 1970, "Annular flow of two immiscible liquids I. Mechanisms," *The Canadian Journal of Chemical Engineering*, 48(5), pp. 514-520.
- [40] Brauner, N., 1991, "Two-phase liquid-liquid annular flow," *International journal of multiphase flow*, 17(1), pp. 59-76.
- [41] Sotgia, G., Tartarini, P., and Stalio, E., 2008, "Experimental analysis of flow regimes and pressure drop reduction in oil–water mixtures," *International Journal of Multiphase Flow*, 34(12), pp. 1161-1174.
- [42] Angeli, P., and Hewitt, G., 1999, "Pressure gradient in horizontal liquid–liquid flows," *International journal of multiphase flow*, 24(7), pp. 1183-1203.
- [43] Kashid, M., and Kiwi-Minsker, L., 2011, "Quantitative prediction of flow patterns in liquid–liquid flow in micro-capillaries," *Chemical Engineering and Processing: Process Intensification*, 50(10), pp. 972-978.
- [44] Brauner, N., Maron, D. M., and Rovinsky, J., 1998, "A two-fluid model for stratified flows with curved interfaces," *International journal of multiphase flow*, 24(6), pp. 975-1004.
- [45] Dreyfus, R., Tabeling, P., and Willaime, H., 2003, "Ordered and disordered patterns in two-phase flows in microchannels," *Physical review letters*, 90(14), p. 144505.
- [46] Wlodkowic, D., and Darzynkiewicz, Z., 2011, "Rise of the micromachines: microfluidics and the future of cytometry," *Methods in cell biology*, 102, p. 105.
- [47] Oliemans, R., and Ooms, G., 1986, "Core-annular flow of oil and water," *Multiphase science and technology*, 2(1-4).
- [48] Lee, C. Y., and Lee, S. Y., 2008, "Pressure drop of two-phase plug flow in round mini-channels: influence of surface wettability," *Experimental Thermal and Fluid Science*, 32(8), pp. 1716-1722.
- [49] Thome, J. R., El Hajal, J., and Cavallini, A., 2003, "Condensation in horizontal tubes, part 2: new heat transfer model based on flow regimes," *International Journal of Heat and Mass Transfer*, 46(18), pp. 3365-3387.
- [50] Munson, B. R., Young, D. F., and Okiishi, T. H., 2006, "Fundamentals of Fluid Mechanics, John Wiley & Sons," Inc., USA.
- [51] da Silva, R. C. R., Mohamed, R. S., and Bannwart, A. C., 2006, "Wettability alteration of internal surfaces of pipelines for use in the transportation of heavy oil via core-flow," *Journal of Petroleum Science and Engineering*, 51(1), pp. 17-25.

# Appendix A - Fluid Properties



2780 Waterfront Pkwy, E. Dr. Suite 200 Indianapolis, IN 46214  
 Phone 317-328-5683 Fax 317-328-5683 Sales 1-800-437-3188 www.calumetspecialty.com

## Certificate of Analysis

PO Number: MD-4132015	Order Number: 221038
Date Ordered: 04/20/2015	Shipping Date: 04/23/2015
Tanker/Cmpt: /0	Lot Number: 201504140002
Seal # List:	Date of Mfr: 04/17/2015
Carrier: UPS FRT	Product: PAROL@ 70
Weight Ticket No:	Product Code: PEN1630-00-C-DR
Carrier Ticket No:	Qty: 1.0000 DR

<u>Billing:</u> KANSAS STATE UNIVERSITY 3002 RATHBONE HALL ATTN DERBY MANHATTAN, KS 66506	<u>Shipping To:</u> KANSAS STATE UNIVERSITY 3002 RATHBONE HALL MANHATTAN, KS 66506-5200	<u>Shipping From:</u> Calumet Specialty Products Partners L.P. 138 PETROLIA ST KARNES CITY, PA 16041
---	--	---

Test Description	Units	Method	Min.	Max.	Results
VISCOSITY @ 40°C	cSt	D445	10.80	13.60	11.67
VISCOSITY @ 100°F	SUS	D2161	65.0	75.0	68.9
API GRAVITY @ 60°F		D4052			35.9
SPECIFIC GRAVITY @ 60/60°F		D4052			.8455
SPECIFIC GRAVITY @ 25/25°C		D4052	.8330	.8610	.8412
FLASH POINT, COC	°F	D92			395
COLOR, SAYBOLT		D156	30		30
FDA 21 CFR 178.3620(B)	P/F	FDA	PASS		PASS

Analysis Certified By: Mark Voelker Laboratory Manager Mark J. Seelher  
 Printed Name Title

Figure A-1: Parol 70 oil Manufacture data sheet



2780 Waterfront Pkwy. E. Dr. Suite 200 Indianapolis, IN 46214  
 Phone 317-328-5660 Fax 317-328-5668 Sales 1-800-437-3188 www.calumetspecialty.com

### Certificate of Analysis

PO Number: MD-4132015	Order Number: 221038
Date Ordered: 04/20/2015	Shipping Date: 04/23/2015
Tanker/Cmpt: /0	Lot Number: 201504070008
Seal # List:	Date of Mfr: 04/22/2015
Carrier: UPS FRT	Product: PAROL@ 100
Weight Ticket No:	Product Code: PEN1650-00-C-DR
Carrier Ticket No:	Qty: 1.0000 DR

<u>Billing:</u> KANSAS STATE UNIVERSITY 3002 RATHBONE HALL ATTN DERBY MANHATTAN, KS 66506	<u>Shipping To:</u> KANSAS STATE UNIVERSITY 3002 RATHBONE HALL MANHATTAN, KS 66506-5200	<u>Shipping From:</u> Calumet Specialty Products Partners L.P. 138 PETROLIA ST KARNS CITY, PA 16041
---	--	--

Test Description	Units	Method	Min.	Max.	Results
VISCOSITY @ 100°F	SUS	D2161	100.0	115.0	109.1
VISCOSITY @ 40°C	cSt	D445			20.80
API GRAVITY @ 60°F		D4052			34.6
SPECIFIC GRAVITY @ 25/25°C		D4052			.8476
FLASH POINT, COC	*F	D92			430
COLOR, SAYBOLT		D156	25		30
FDA 21 CFR 178.3620(B)	P/F	FDA	PASS		PASS

Analysis Certified By: Merk Voelker Laboratory Manager Mark J. Walker  
 Printed Name Title

**Figure A-2: Parol 100 oil Manufacture data sheet**